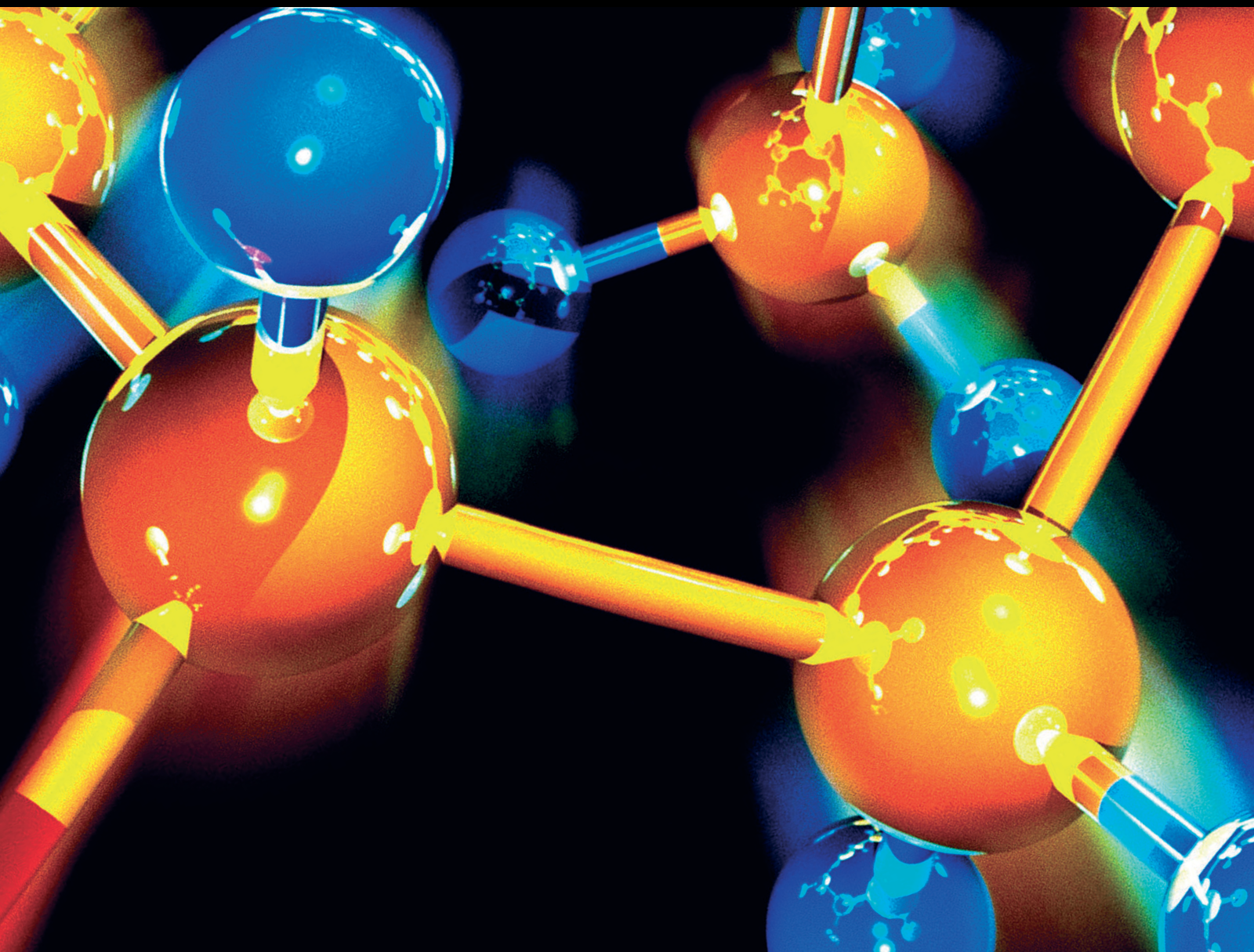


Advanced Materials for Clean Water: Removal of Pollutants and Biological Assessment of Water

Lead Guest Editor: Hassan Ait Ahsaine

Guest Editors: Abdeljalil Benhachemi, Mohamed Zbair, and Ioannis Anastopoulos



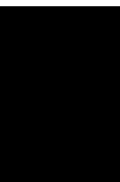


**Advanced Materials for Clean Water: Removal
of Pollutants and Biological Assessment of
Water**

**Advanced Materials for Clean Water:
Removal of Pollutants and Biological
Assessment of Water**

Lead Guest Editor: Hassan Ait Ahsaine

Guest Editors: Abdeljalil Benlhachemi, Mohamed
Zbair, and Ioannis Anastopoulos



Copyright © 2019 Hindawi Limited. All rights reserved.

This is a special issue published in "Journal of Chemistry." All articles are open access articles distributed under the Creative Commons Attribution License, which permits unrestricted use, distribution, and reproduction in any medium, provided the original work is properly cited.

Chief Editor

Kaustubha Mohanty, India

Associate Editors

Mohammad Al-Ghouti, Qatar


Tingyue Gu , USA

Teodorico C. Ramalho , Brazil

Artur M. S. Silva , Portugal

Contents

Eco-Friendly Photocatalyst Derived from Egg Shell Waste for Dye Degradation

Achala Amarasinghe and Dakshika Wanniarachchi 

Research Article (13 pages), Article ID 8184732, Volume 2019 (2019)

Preparation, Characterization, and Application of Metakaolin-Based Geopolymer for Removal of Methylene Blue from Aqueous Solution

Marouane El Alouani , Saliha Alehyen, Mohammed El Achouri, and M'hamed Taibi

Research Article (14 pages), Article ID 4212901, Volume 2019 (2019)

Research Article

Eco-Friendly Photocatalyst Derived from Egg Shell Waste for Dye Degradation

Achala Amarasinghe¹ and Dakshika Wanniarachchi ²

¹Department of Science and Technology, Uva Wellassa University, Badulla, Sri Lanka

²Instrument Center, Faculty of Applied Sciences, University of Sri Jayewardenepura, Nugegoda, Sri Lanka

Correspondence should be addressed to Dakshika Wanniarachchi; dakshikacw@sjp.ac.lk

Received 14 June 2019; Revised 14 August 2019; Accepted 16 August 2019; Published 26 September 2019

Guest Editor: Hassan Ait Ahsaine

Copyright © 2019 Achala Amarasinghe and Dakshika Wanniarachchi. This is an open access article distributed under the Creative Commons Attribution License, which permits unrestricted use, distribution, and reproduction in any medium, provided the original work is properly cited.

This study is focused on removal of dyes in water bodies using calcined egg shell powder obtained from waste egg shells as a new material for photocatalytic dye removal. The photocatalytic activity of calcined egg shell powder (CESP) was compared with the raw egg shell powder (RESP) under light and dark conditions. The results reveal that CESP has significantly a higher dye degradation capability of 80% compared to the RESP which is 20% under the same condition. Furthermore, under light conditions, CESP has shown nearly 50% increase in dye degradation compared to the same material in the dark. The kinetics of dye degradation follows pseudo-second-order kinetics suggesting the chemisorption process and the Freundlich adsorption isotherm is best fitted (R^2 value is 0.96 for the linear fit) with the dye adsorption process. The application of CESP in industry is studied with a textile acid dye Lanasyne Rez F5B, and the results reveal it follows pseudo-second-order kinetics in dye removal.

1. Introduction

Colour is a major parameter considered when defining the quality of water. Colour of water is often changed due to dissolved or suspended solids. Naturally, colour of water can be changed due to tannings from decomposing leaves or mud on a rainy day. However, water bodies are polluted because of the release of improperly treated industrial waste containing various dyes and pigments. These could prevent penetration of sunlight into the bottom of rivers and lakes causing a decrease in dissolved oxygen content and threat to aquatic plants and animals in threat. Furthermore, dyes and degraded by-products of dyes are toxic and carcinogenic [1, 2].

The removal methods available for textile dyes can be classified as physical methods, biological methods, and chemical methods [3]. Physical methods often consider adsorption of a dye on to a suitable sorbent. Here, activated carbon is the most efficient in removing variety of dyes [4]. However, it has limitation in application due to the high cost and material loss during regeneration [3]. Consequently,

there are some low-cost sorbents introduced with biological origin as alternatives [4–8]. Apart from physical methods, biological treatments include use of algae or bacteria to metabolize decomposition of dyes. [9, 10]. Conversely, most of the dyes are designed to give a long-lasting colour to the textile. Therefore, degradation of these dyes requires advanced chemical oxidation methods. Some of the most studied and used oxidants are ozone [11] and hydrogen peroxide in the presence of UV light. The Fenton process is also used in degradation of textile dyes [12]. All these methods utilize highly reactive radical species of oxygen or hydroxyl to breakdown the dye [12–14]. However, these reactive oxygen species are short lived; hence, industrial application of hydrogen peroxide is limited. There are novel methods emerging in situ generation of hydrogen peroxide/hydroxyl radical for more viable use [12, 15]. Metal oxides such as titanium oxide [16–18] and zinc oxide [19, 20] are widely studied and used in degradation of dye materials photocatalytically. The inherent problems which limit the use of TiO_2 is the band gap which is ~ 3.2 eV and requires UV light to operate as a photocatalyst [21]. Studies are extended

to include composites of TiO₂ or ZnO with other metal oxides aiming higher degradation efficiency and photocatalytic activity using visible light [21–25].

There is constant search for novel photocatalysts other than traditional TiO₂- or ZnO-based catalysts. In recent years, there have been number of studies conducted on calcium-based photocatalysts such as calcium hydroxyapatite [26] and calcium antimony oxide hydroxide [27] for dye degradation. In addition, calcium hydroxide is also used as a catalyst for transesterification in biodiesel production [28]. Although there are many alternatives for calcium sources, egg shells can be utilized as it is available in abundant [29] and often considered as a waste material which is discarded without further use. The current trends to use egg shell waste are in agriculture as a fertilizer or as animal feed [30]. The anatomy of egg shell indicates the presence of pores which facilitate air exchange for the growing embryo [31]. Therefore, this material serves as an effective surface for dye adsorption processes. There have been studies conducted for the use of egg shell powder and egg shell membrane for dye removal [32–38]. Furthermore, egg shell powder has been used to develop several composite materials for dye removal incorporating TiO₂, polymer, and clay materials [39–42]. There is a significant enhancement in dye removal activity observed for egg shell powder composites compared to egg shell powder alone [39–42].

However, the dye removal capability of egg shell powder which is thermally treated above the thermal decomposition temperature (830°C) is not studied so far. Also, the photocatalytic activity is not well established for the calcined egg shell powder (CESP). Therefore, the main focus of this paper is to evaluate the dye removal efficiency of CESP as an adsorbent and as a photocatalyst. The term calcination is defined as the heating of a substance to high temperature allowing oxidation and release of any volatile substances [43]. In many papers, calcined egg shell powder indicates well purified and dried egg shell powder (100–120°C) [36]. However, in this paper, the “calcined egg shell powder (CESP) denotes egg shell powder heated at 900°C which is above the decomposition temperature of calcium carbonate.

Dye removal efficiency and photocatalytic dye degradation of the two materials were compared using methylene blue as the model dye. The dye adsorption processes are studied with the Langmuir and Freundlich isotherms, and rates were evaluated as first-order and pseudo-second-order kinetics. Furthermore, dye removal capacity of textile acid dye Lanasin F5B was studied as an application of the CESP in industrial dye removal.

2. Materials and Methods

2.1. Materials and Chemicals. Egg shells were obtained from the university cafeteria. Methylene blue (Merck limited, India) and industrial dye (Lanasin Rez F5B) (Riddhi Siddhi Trading Co. Maharashtra, India) were purchased and used as received.

2.2. Calcined Egg Shell Powder Preparation. Egg shells were collected from the university cafeteria and cleaned with

distilled water thoroughly to remove all the unnecessary materials adhered to the egg shells. Then, egg shells were dried at 120°C in the oven for 24 hours. Dried egg shells were ground and calcined in a muffle furnace (HD-230 “PAD,” Forns Hobersal SL, Barcelona) under static air conditions at 900°C to produce CESP for 3 hrs.

2.3. Calcined Egg Shell Powder Characterization. Characterization of CESP and RESP was done by Fourier-transform infrared (FTIR, Bruker, Alpha) and X-ray diffraction (Rigaku Ultima IV) (S1.Tables 1–4 for supporting information regarding experimental conditions).

2.4. Photocatalytic Experiments. The photocatalytic activity of CESP and RESP was compared by evaluating dye removal efficiencies of solutions with dye and egg shell powder under the dark and light conditions. The removal efficiency of calcined egg shell powder and raw egg shell powder was calculated by taking 0.50 g of each powder dispersed in MB solutions (50 ml, 10 mg/l) in a glass stoppered bottle. Then, for each type of powder, one solution was kept under light condition, while the other solution was kept under dark condition for 2 hrs. Light condition was provided by 23 W of fluorescent bulb inside a light box. Solutions were centrifuged, and absorbance was measured using the UV-visible spectrophotometer (GENESYS, Thermo Scientific) every 30 minutes. Each experiment was conducted in triplicate. Removal efficiency was calculated by using equation (1). Removal efficacies were repeated for CESP under light conditions in triplicate and in the dark for two hours and 9 hrs. RESP study was repeated for 2 hrs and 9 hrs duration (S2.Tables 1 and 2 and S3.Tables 1 and 2 and S3.Figures 1 and 2 for supporting information regarding experimental conditions):

$$\eta = \frac{(C_0 - C_f)}{C_0} * 100, \quad (1)$$

where η is the removal efficiency, C_0 is the initial MB concentration (mg/l), and C_f is the MB concentration at equilibrium (mg/l).

2.5. Adsorption Experiments. Adsorption studies were conducted for CESP (0.50 g) placed in a glass stoppered bottle with 50 ml solutions of MB aqueous solutions (4 mg/l, 6 mg/l, 8 mg/l, 10 mg/l, 12 mg/l, 14 mg/l, 16 mg/l, 18 mg/l, and 20 mg/l). These solutions were studied under the light conditions. Then, absorbance measurement of each solution was obtained after 28 hrs. Amount of dye adsorbed and degraded at the equilibrium (q_e) was calculated by equation (2) for Langmuir and Freundlich isotherms. A control experiment was conducted in parallel without the CESP. Experiment was repeated twice:

$$q_e = \frac{(C_0 - C_e) * V}{W}, \quad (2)$$

where q_e is the amount of MB adsorbed at the equilibrium (mg/g), C_0 is the initial MB concentration (mg/l), C_e is the

MB concentration at equilibrium (mg/l), V is the volume of the solution (L), and W is the mass of the dry adsorbent (g) (S4.Figures 1–4 for supporting information regarding repeated trials for isotherms fitting):

2.6. Kinetic Studies. CESP (0.50 g) was dispersed in MB solution (10 mg/l, 50 ml). One solution was used as the control without exposing to light by covering it with an aluminium foil. All samples were kept under the 23 W fluorescent bulb for 2 hrs inside the light box. Absorbance of each sample was measured at 15-minute intervals. The amount of MB adsorbed from the solutions at various time intervals was calculated by equation (3). Same procedure was followed for RESP. The experiment was conducted in triplicate:

$$q_t = \frac{(C_0 - C_t) * V}{W}, \quad (3)$$

where q_t is the amount of MB adsorption at time t (mg/g), C_0 is the initial MB concentration (mg/l), C_t is the concentration of MB at any time t (mg/l), V is the volume of the solution (L), and W is the dry mass of the adsorbent (g).

2.7. Removal Efficiency of Industrial Dye. The removal efficiency of industrial dye was studied using 50 mg/l, 60 mg/l, 70 mg/l, 80 mg/l, 90 mg/l, and 100 mg/l of industrial dye solutions. Maximum absorbance wavelength of the industrial dye was 530 nm. Adsorption isotherms were developed using 1.5 g of CESP dispersed in 25 ml of 50 mg/l, 60 mg/l, 70 mg/l, 80 mg/l, 90 mg/l, and 100 mg/l dye solutions. Then, absorbance of these solutions was measured after keeping them under the light condition for 28 hours to calculate q_e . Kinetic experiments were conducted for 25 ml of 100 mg/l industrial dye solutions with 1.5 g of CESP. These solutions were kept under light for 2 hours, and absorbance of samples was measured for every 15 minutes.

3. Results and Discussion

3.1. Sample Characterization. According to the data of XRD illustrated in Figures 1(a) and 1(b), crystalline calcite in RESP and calcium hydroxide in CESP are present. Therefore, it is clear that calcium carbonate in raw egg shell powder has been transformed into the calcium oxide at 900°C. But due to exposure to the atmosphere, it is converted to calcium hydroxide. The presence of narrower peaks indicates that CESP and RESP are crystalline. The size of the crystallite is calculated using Debye–Scherrer’s formula [44] considering crystals spherical with cubic symmetry ($K=0.94$) for Cu-K α wavelength (1.5406 Å) for peak between 2θ values 30 deg. to 60 deg.

Accordingly, the average crystallite size of RESP is about 30–45 nm and that of CESP is about 15–23 nm.

Tsai et al [45] have characterized RESP with FTIR spectroscopy. The FTIR spectrum of RESP (Figure 2) indicates presence of organic matter corresponding to C-H vibration peaks at 2969 cm^{-1} , 2875 cm^{-1} , and 2527 cm^{-1} . These FTIR bands are absent in egg shell powder calcined at

900°C, indicating decay of organic matter. The peak at 1416 cm^{-1} , 879 cm^{-1} , and 705 cm^{-1} is related to the carbonate anion [45, 46]. Furthermore, the band at 515 cm^{-1} for CESP indicate the OH band and for the calcium oxide band. According to the XRD data and FTIR data, further confirmation is provided for the transformation of calcium oxide to calcium hydroxide.

3.2. Comparison of Removal Efficiencies and Photocatalytic Activity. The removal efficiencies of MB were studied with raw egg shell powder and calcined egg shell powder recording UV-Visible spectra every 30 minutes under dark conditions. The UV-visible spectrum of MB clearly indicates a decrease of the band at 665 nm as MB is adsorbed into egg shell powder, as illustrated in Figures 3(a) and 3(b).

Figures 3(a) and 3(b) represent the absorbance curves of MB due to RESP and CESP, respectively. MB concentration of both solutions has been reduced gradually within 2 hours. But absorbance curves of MB solution with CESP indicate blue shift of the band at around 560 nm after 75 minutes. But this is absent in the solution of MB-RESP, and only reducing absorbance curve is observed. If only adsorption is the process which was proceeding in the experiment, reducing curves must be generated without any movement of curves. This suggests another reaction is the reason for the shifting of this curves.

Egg shell is designed by nature to give protection to the embryo from harmful attacks of bacteria other factors. A thin layer of the protein matrix is bonded to the egg shell containing calcite. The egg shell has many pores to allow exchange of gaseous products and water for healthy growth of the embryo [31]. Therefore, decrease in MB concentration in solution observed in raw egg shell powder and calcined egg shell powder under dark could be due to physical adsorption, which is in accordance with the work of Tsai and coworkers [32, 45]. Furthermore, the work of El-Kemary and coworkers on TiO₂/egg shell nanocrystals reported increasing removal efficiency when the calcination temperature is increased from 400°C to 900°C for the acid red nylon 57 dye [39]. Therefore, the enhanced dye degradation of CESP compared to RESP is in agreement with the above data.

The photocatalytic activity was studied for RESP and for CESP. Figures 4(a) and 4(b) indicate the absorbance curve of MB solutions with RESP and CESP in the presence of visible light. Figure 4(b) clearly indicates a degradation reaction proceeding in the solution with CESP. In the presence of light, even at the beginning, the absorbance curve has been blue shifted. But these changes are not observed in the solution with the RESP. Only deducing curves can be observed. The solution with CESP indicates reduction of MB concentration, and bands of the absorbance curves after 105 minutes have been changed significantly, shifting the maximum absorbance towards 615 nm. However, Figure 3(b) (dark condition) indicates small shifting of curves with comparison to Figure 4(b) (light condition). Studies of Yang et al. on photocatalytic degradation of MB with the rice husk/TiO₂/SiO₂ catalyst observed rapid degradation of MB in the presence of visible light [47].

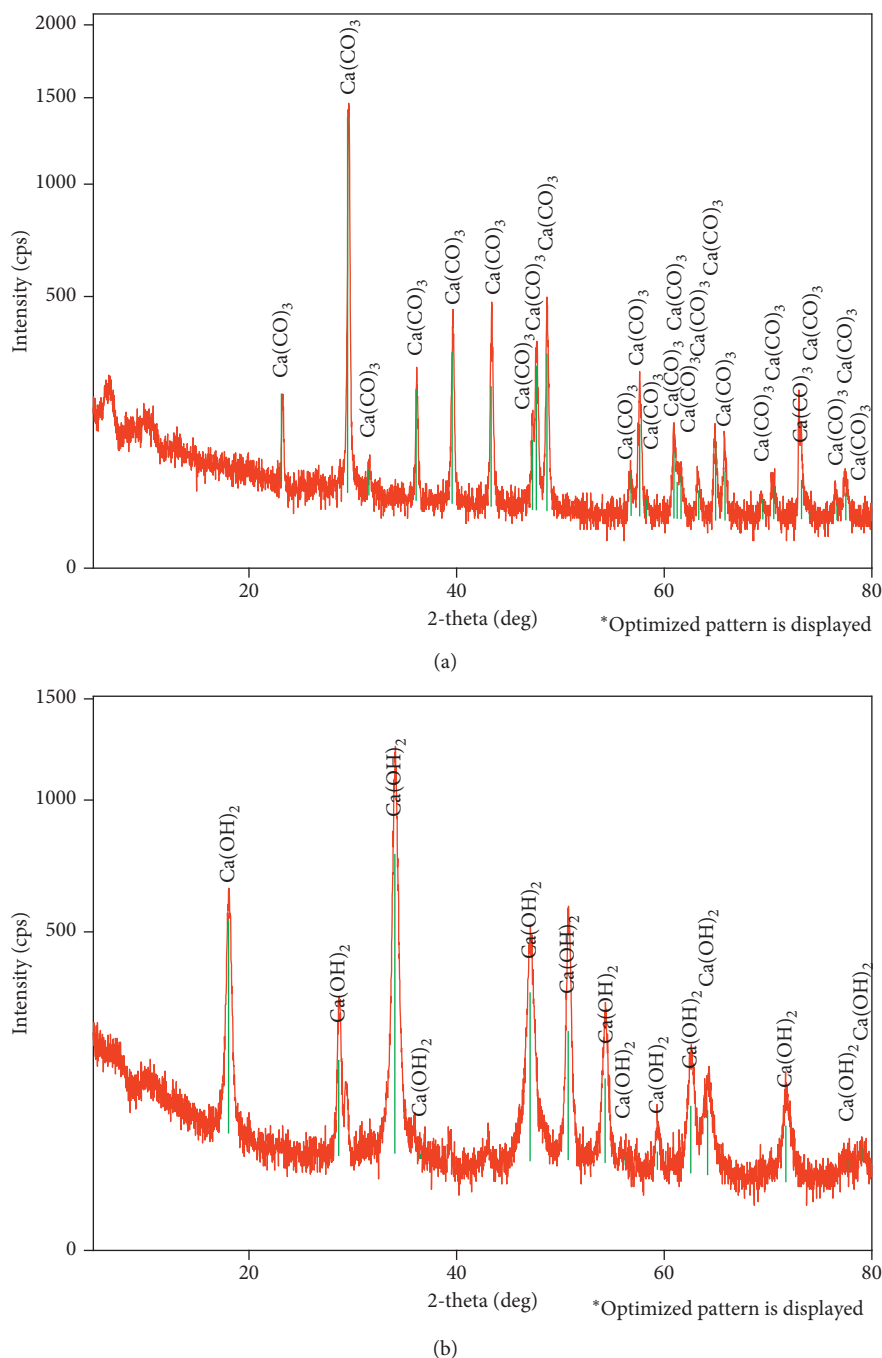


FIGURE 1: X-ray diffraction patterns: (a) raw egg shell powder; (b) calcined egg shell powder.

CESP mainly consists of Ca(OH)_2 which can give basic solution when dissolved in water. Hence, it can be presumed that the reason for the alteration of adsorption bands could be due to the basicity. In order to clarify this fact, absorbance curves of MB solution were measured with different pH values. Figure 5 interprets the absorbance curves of MB at different pH values. The pH value of solutions is adjusted with using HCl and NaOH solutions. According to Figure 5, it is clear that pH alone is not the agent for shift in UV-visible bands in MB solution. However, the pH of the solution is an important factor which decides the surface

potential of the material. In a study where TiO_2 is used as the photocatalyst, it is observed that the dye adsorption and degradation are enhanced in a higher pH value. This is due to the availability of the anionic surface (TiO^- in this case) to bond with the $-\text{C}-\text{S}^+=\text{C}-$ group in MB to initiate degradation of MB producing the sulfone group [48]. Therefore, possibly a similar phenomenon can be suggested for the CESP.

Removal efficiency of MB was calculated for both RESP and for CESP. Figures 6(a) and 6(b) compare the removal efficiencies of MB under dark and light conditions for both types of egg shell powders. In the presence of light, removal

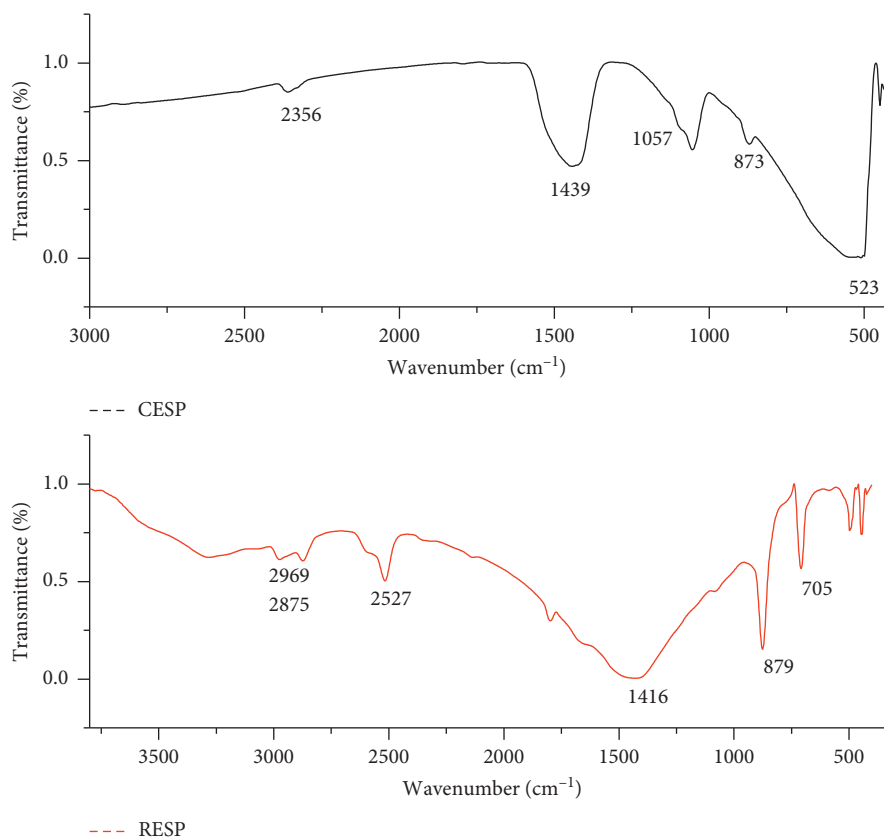


FIGURE 2: FTIR spectra of raw egg shell powder and calcined egg shell powder.

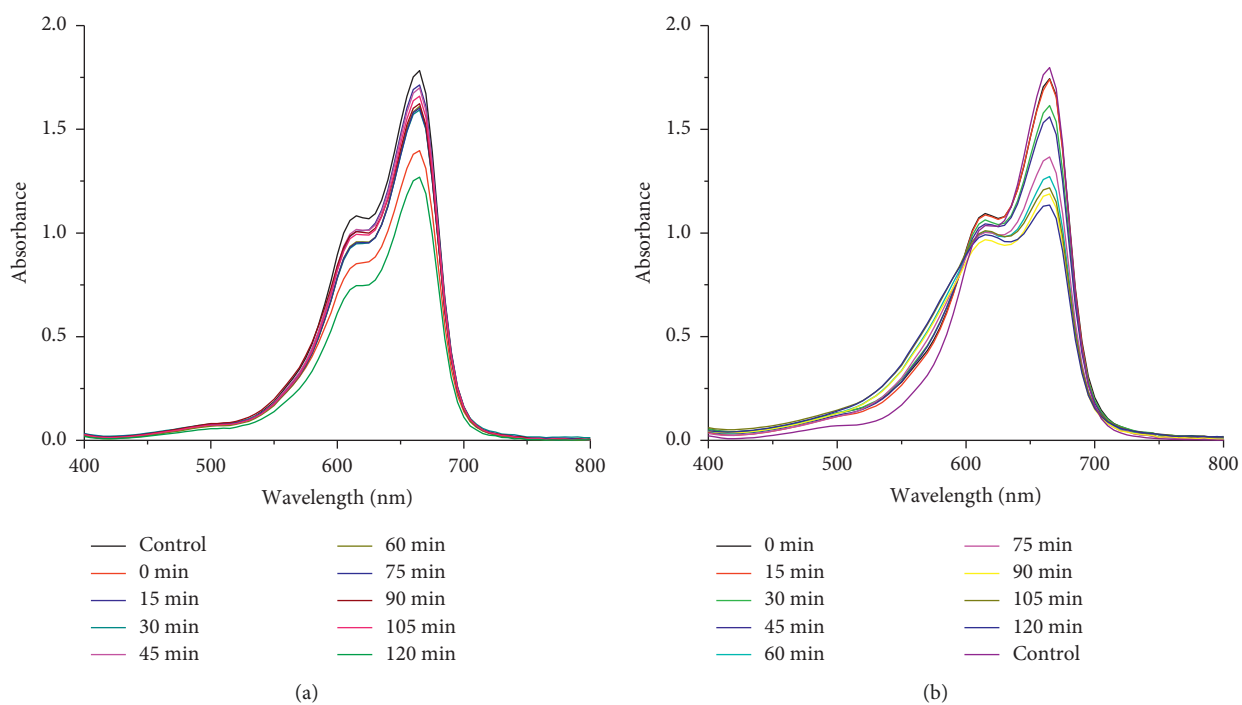
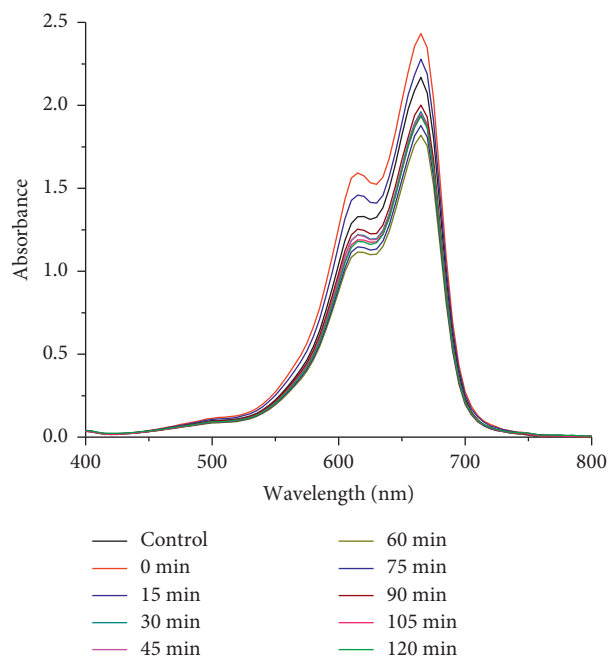


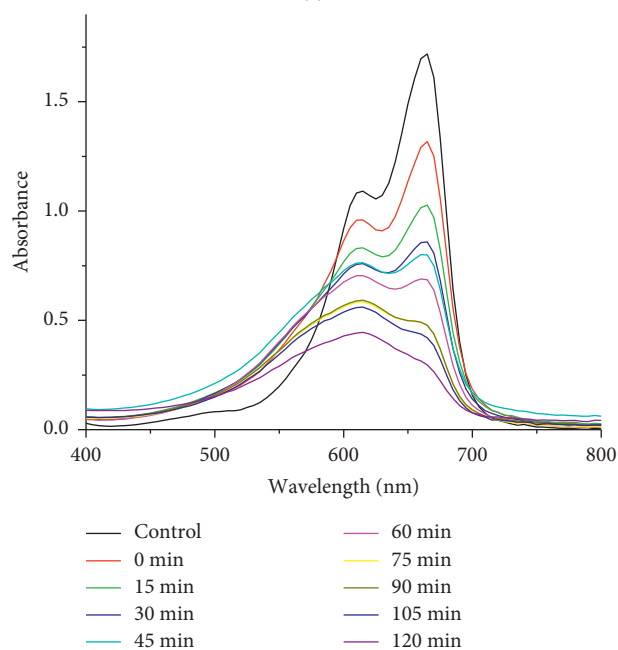
FIGURE 3: Absorbance curves of MB solution (dark): (a) raw egg shell powder; (b) calcined egg shell powder.

efficiency of CESP is higher than RESP. The reported efficiency for CESP after 2 hours is 82%, while that of RESP is 21%. Comparatively, CESP has higher removal efficiency

than RESP under light conditions. Furthermore, when CESP considered, the removal efficiency in the presence of light (82%) is much higher than that in the dark (44%). These



(a)



(b)

FIGURE 4: Absorbance curves of MB solution (light): (a) raw egg shell powder; (b) calcined egg shell powder.

figures clearly interpreted that removal efficiency of MB in the light condition is higher compared to the removal efficiency in the dark condition. The calculated removal efficiencies under dark and light conditions are given in S2.Tables 1 and 2 in the supporting information, respectively.

The removal efficiencies were calculated with standard deviation between 10 and 5%. This suggests a possible degradation pathway involving photocatalytic activity. The semiconductor materials absorb photons from the UV radiation and promote electrons in the valence band to the

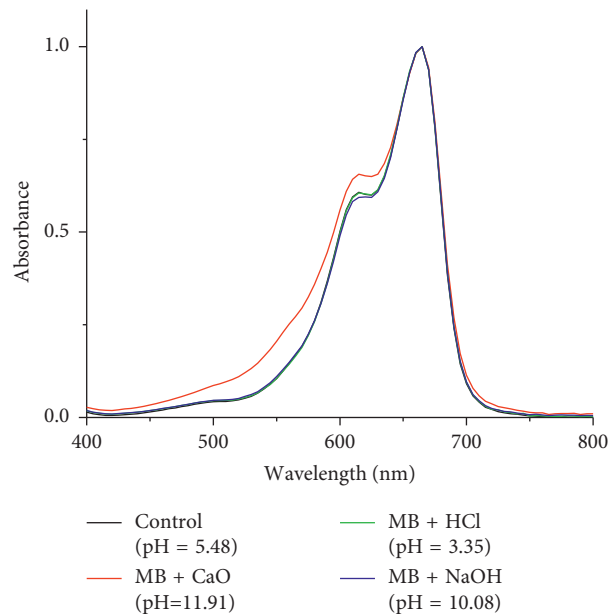


FIGURE 5: Absorbance curves of MB solution in different pH values.

conduction band, creating a hole in the valence band. These excited electrons can react with dye or oxygen to produce the superoxide anion. At the same time, holes in the valence band can also react with water molecules to produce hydroxyl radical. Consequently, the presence of reactive oxygen species leads to degradation of dye [17]. RESP consists of mainly CaCO_3 , and CESP has $\text{Ca}(\text{OH})_2$. The reported band gap of these materials is 5.07 eV [29] and 5.7 eV [49, 50], respectively. These band gaps suggest photocatalytic activity under visible light conditions is hardly possible. However, studies of Zang et al. suggest observed band gap for $\text{Ca}(\text{OH})_2$ is further reduced to 3.2 eV subtracting energy gap between bottom of the conduction band to the Fermi level (2.5 eV) from the band gap of conduction and valence (5.7 eV) [49]. This allows excitation wavelength around 400 nm; thus, catalyst could be active at the margin of visible radiation.

When photo is excited, MB is converted to cationic dye radical which degrades the by-products. The absorption bands at 665 nm and 615 nm of MB correspond to monomer and dimer units [51, 52]. The decrease in band at 665 nm in the presence of light with calcined egg shell powder suggests rapid degradation of monomer units. In addition, the blue shift observed is due to further degradation of phenothiazine [51]. Furthermore, the study using CESP was continued for more than 9 hrs, and the results reveal over 90% efficiency of MB removal under light conditions end of first 180 min, while it was only 65% under dark conditions. The recorded UV-visible spectra for long exposure study under light and dark conditions are given under supporting information S3.Figures 1 and 2. The efficiencies and maximum amount removed (q_{max}) are given in S3.Tables 1 and 2, respectively.

3.3. Kinetic Experiments for CESP and RESP. The kinetic behaviour of the dye degradation was studied with pseudo-first-order and pseudo-second-order kinetics to evaluate the

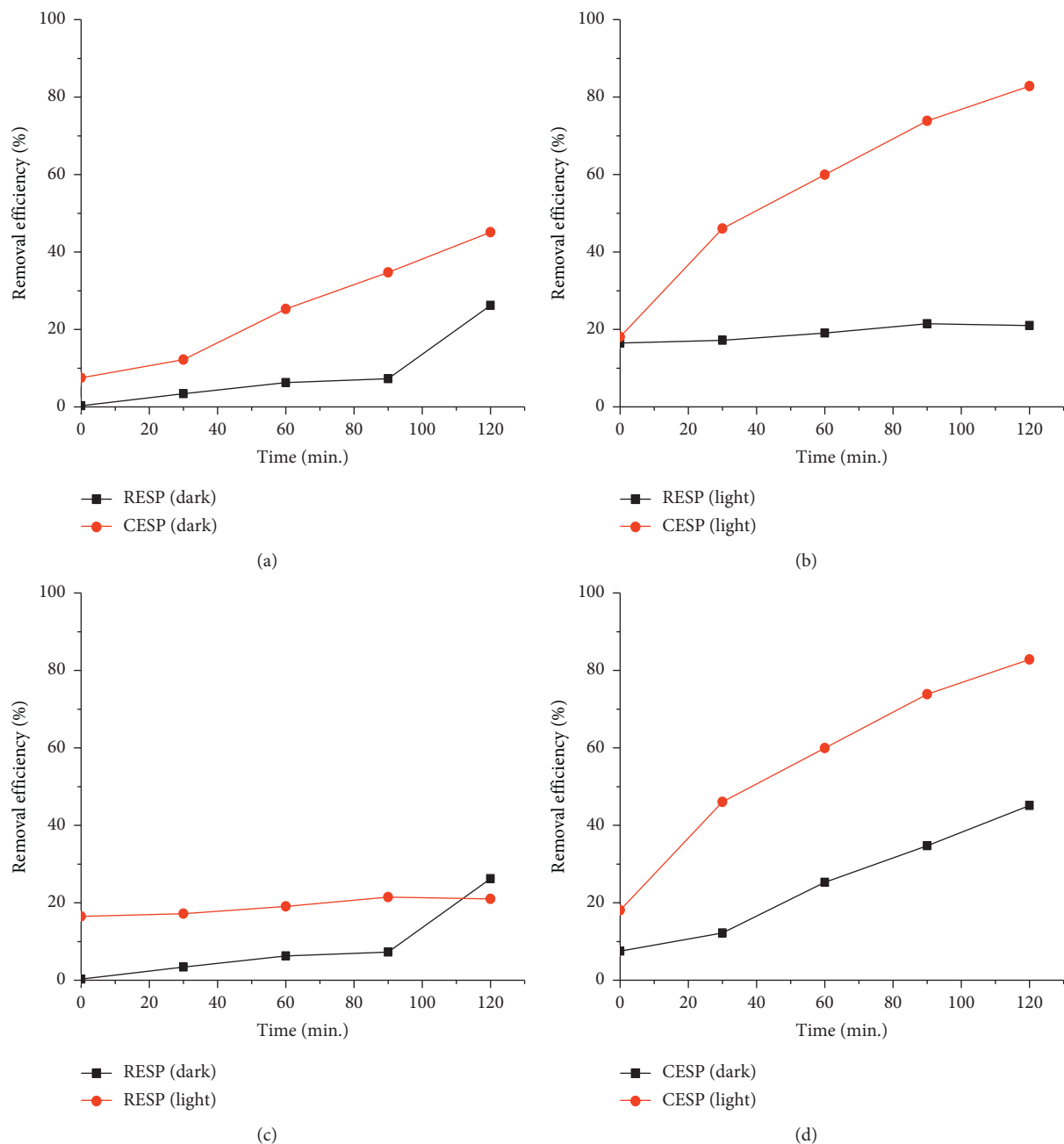


FIGURE 6: Removal efficiencies of MB in raw egg shell powder and calcined egg shell powder.

photocatalytic effect. The first-order and second-order kinetic models are given in equations (4) and (5).

First-order kinetic model equation [53]:

$$\frac{1}{q_t} = \frac{1}{q_1} + \frac{k_1}{q_1} \left[\frac{1}{t} \right], \quad (4)$$

where q_t and q_1 are the amount of dye adsorbed at time t and at equilibrium (mg/g) and k_1 is the first-order kinetic rate constant.

Second-order kinetic model [53]:

$$\frac{t}{q_t} = \frac{1}{k_2 q_2^2} + \frac{1}{q_2} t, \quad (5)$$

where q_2 is the maximum adsorption capacity, q_t is the adsorbed amount at time t ($\text{mg}\cdot\text{g}^{-1}$), and k_2 is the equilibrium rate constant for pseudo-second-order kinetic ($\text{g}\cdot\text{mg}^{-1}\cdot\text{min}^{-1}$).

Kinetic modes for MB on to the CESP are shown in Figures 7(a) and 7(b). When correlation coefficient values of pseudo-first-order and pseudo-second-order are compared, the R^2 value of pseudo-second-order is higher than the pseudo-first-order value. Therefore, pseudo-second-order kinetic is the best fitted kinetic model for MB on to the CESP. The kinetic study was conducted for the RESP in the same way, and RESP also follows pseudo-second-order kinetic model which is in agreement with Tsai and coworkers [32, 45] for MB adsorption on to egg shell powder. Since

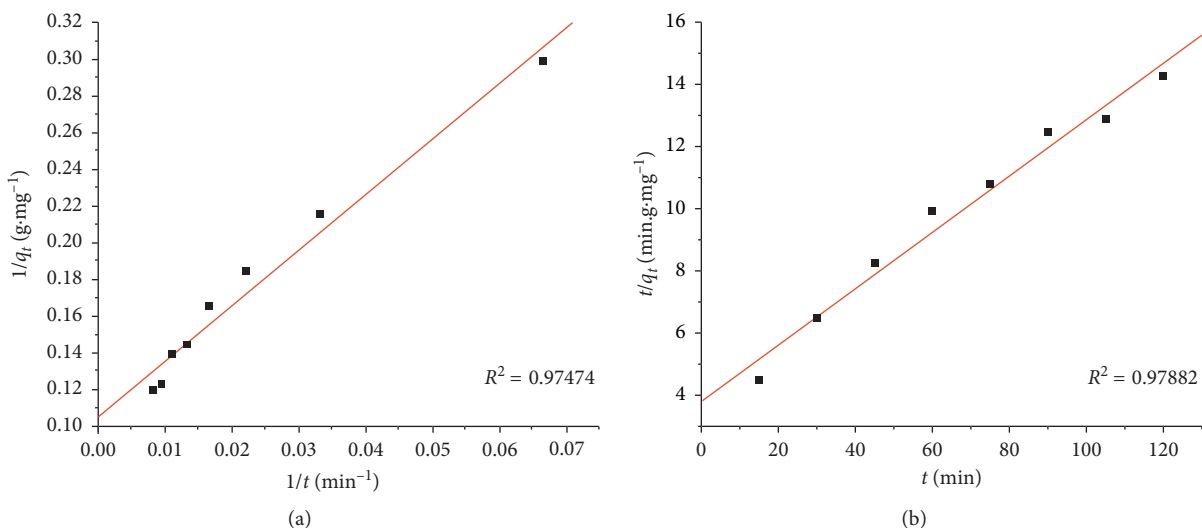


FIGURE 7: (a) First-order kinetics; (b) pseudo-second-order kinetics.

both CESP and RESP indicate pseudo-second-order kinetics, it is possible that the rate limiting step could be bimolecular and chemisorption governs the adsorption process [54]. According to the results, CESP has higher adsorption capacity (11.025 mg.g⁻¹) compared to the RESP (0.23 mg.g⁻¹). Table 1 provides comparison of kinetic study for both types of powders.

3.4. Adsorption Isotherms for Calcined Egg Shell Powder. The adsorption capacities of MB on to CESP were evaluated using the Freundlich isotherm and Langmuir isotherm [53]. The linear forms of these isotherms are given in equations (6) and (7).

Langmuir isotherm:

$$\frac{C_e}{q_e} = \frac{1}{q_{\max} K_L} + \frac{C_e}{q_{\max}}, \quad (6)$$

where q_e is the equilibrium concentration on the calcium oxide (mg/g), C_e is the equilibrium concentration in the solution (mg/l), q_{\max} is the monolayer adsorption capacity of the calcined egg shell powder, and K_L is the Langmuir constant (l/mg).

Freundlich isotherm:

$$\log q_e = \log K_f + \frac{1}{n} \log C_e, \quad (7)$$

where q_e is the equilibrium concentration on the calcium oxide (mg/g), C_e is the equilibrium concentration in the solution (mg/l), and K_f (l/g) and n are Freundlich constants.

According to Figures 8(a) and 8(b), Freundlich isotherm has a high R^2 value than the Langmuir isotherm. Therefore, the Freundlich isotherm is fitted better than the Langmuir isotherm. When Freundlich constant n gets some value other than 1, it gives a parabolic shape for the Freundlich isotherm. The value of n observed for calcined egg shell powder is one, suggesting a linear adsorption of the dye. These linear Freundlich graphs are vital in the industrial applications because linear adsorption provides direct applications for

water treatment industries via direct calculations. Linear adsorption Freundlich graph can be used for calculation of dosage of adsorbent that should be added for maximum removal of the dye from the solution. Furthermore, the Freundlich adsorption isotherm suggests monolayer adsorption of the dye on the surface of calcined egg shell powder, thus facilitating the photocatalytic activity. Tsai and coworkers have studied the adsorption isotherm models for raw egg shell powder with MB. They have observed that the Freundlich isotherms fit more than Langmuir isotherms similar to the results obtained here [32, 45].

3.5. Removal of Industrial Dye Using Calcined Egg Shell Powder. Lanasyne F5B is an acid dye widely used in textile industry. The UV-visible spectra of the industrial dye and removal efficiencies at different time periods are given in S5.Figure 1 and S5.Table 1. The removal of this dye using CESP was studied constructing adsorption isotherms and kinetic studies. According to Figure 9, the industrial dye does not follow linear adsorption with Langmuir isotherm or Freundlich isotherm. The Freundlich adsorption isotherm constant (K_F) for the Lanasyne F5B dye is 0.058 Lg¹, and the Freundlich adsorption isotherm constant (n) is calculated as 0.985. The linear fit for the Freundlich adsorption isotherm is 0.6017 for R^2 suggesting the multilayer adsorption process may proceed with CESP. The industrial dye can be removed with more than 70% efficiency photocatalytically by CESP (S5.Figure 2).

Kinetic studies on this dye removal follow pseudo-second-order kinetics, as illustrated in Figure 9(d), which is comparable to the pseudo-second-order kinetics observed for MB adsorption with CESP. Table 2 provides a summary of adsorption isotherm data and results of kinetic experiments conducted for industrial dye using CESP.

3.6. Comparison of Use of Egg Shell Powder for Removal of Dye. Egg powder has been used to remove several well-known dyes. The studies have been conducted to evaluate

TABLE 1: Summary of kinetic studies for MB removal.

	First-order kinetics			Pseudo-second-order kinetics		
	k_1 (min^{-1})	q_e ($\text{mg}\cdot\text{g}^{-1}$)	R^2	k_2 ($\text{g}\cdot\text{mg}^{-1}\cdot\text{min}^{-1}$)	q_e ($\text{mg}\cdot\text{g}^{-1}$)	R^2
RESP	5.97	0.22	0.63627	0.67	0.23	0.98451
CESP	0.0036	9.53	0.97474	0.0021	11.025	0.97882

Initial MB concentration = 10 mg/l; amount of CESP = 0.5 g.

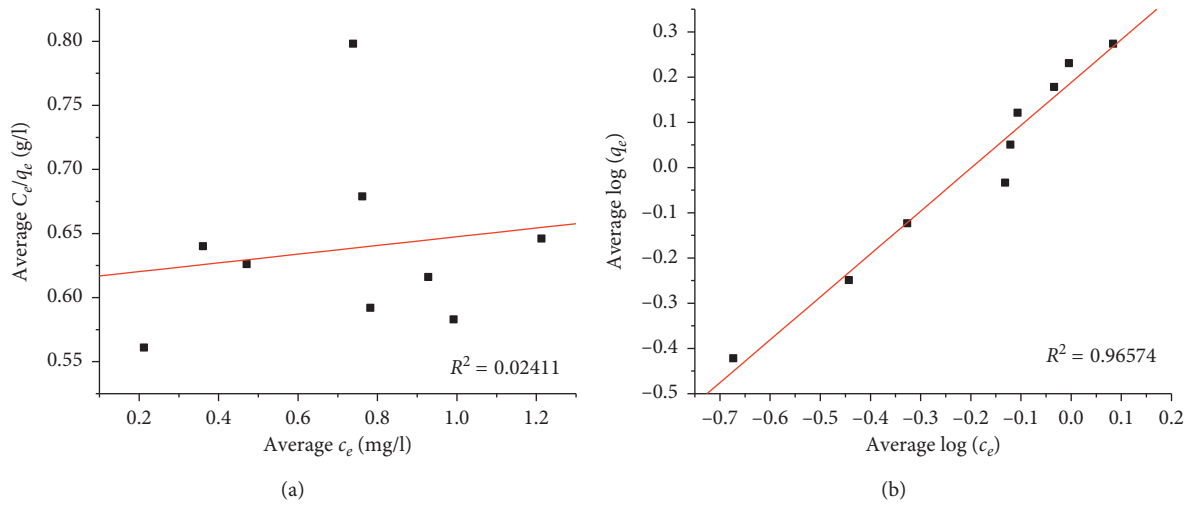


FIGURE 8: (a) Langmuir isotherm and (b) Freundlich isotherm for MB adsorption on to CESP.

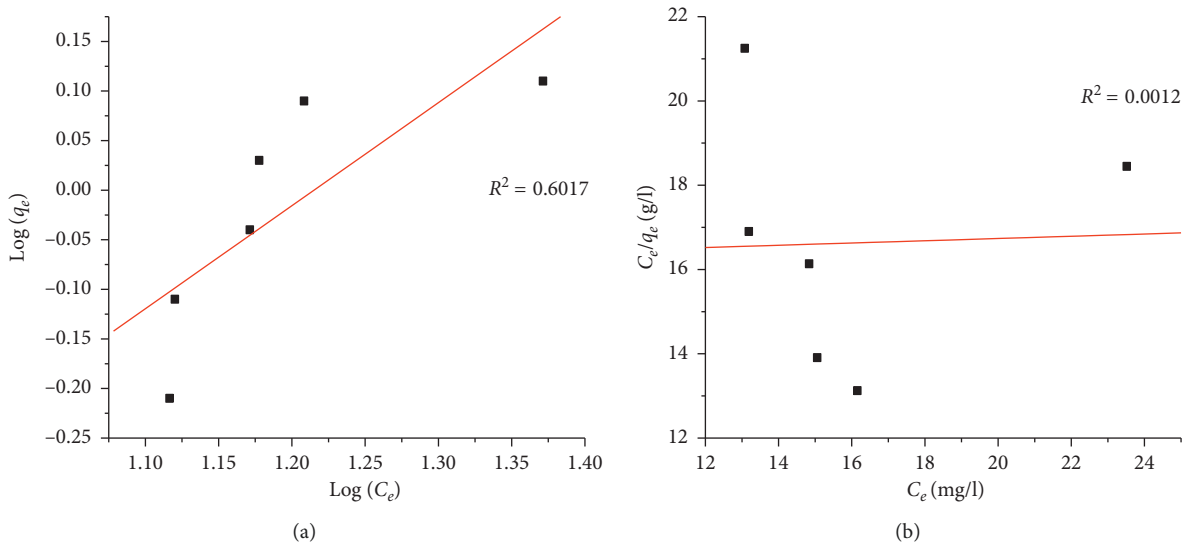


FIGURE 9: Continued.

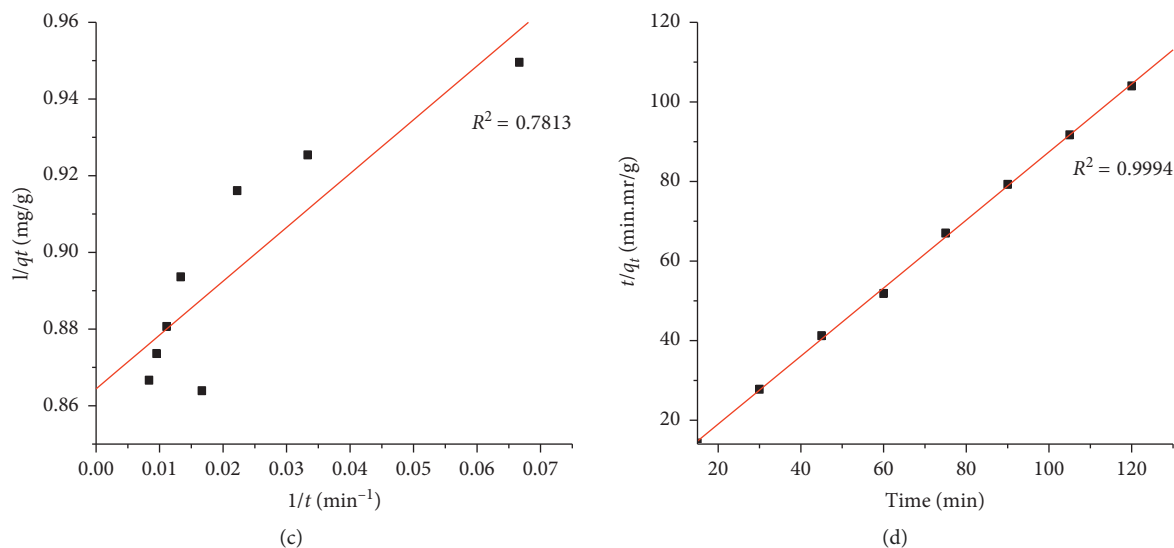


FIGURE 9: (a) Freundlich isotherm; (b) Langmuir isotherm; (c) pseudo-first-order kinetics; (d) pseudo-second-order kinetics.

TABLE 2: Results of kinetic experiments conducted for industrial dye using calcined egg shell powder.

	First-order kinetics			Pseudo-second-order kinetics		
	k_1 (min ⁻¹)	q_e (mg·g ⁻¹)	R^2	k_2 (g·mg ⁻¹ ·min ⁻¹)	q_e (mg·g ⁻¹)	R^2
CESP	1.6241	1.1569	0.7813	0.2933	1.1777	0.9994

Initial MB concentration = 100 mg/l; amount of CESP = 1.5 g.

TABLE 3: Comparison of egg shell powder-, egg shell membrane-, and egg shell powder-based composite materials for dye adsorption.

Adsorbent	Dye	Adsorption capacity (mg/g)	Reference
Egg shell powder	Methylene blue	0.87	[35]
Egg shell powder	Methylene blue	0.8	[45]
Egg shell powder (RESP)	Methylene blue	0.23	This study
Egg shell powder (CESP)	Methylene blue	11.02	This study
Egg shell powder	Congo red	95.25	[33]
Egg shell powder	Rhodamine B	0.14	[34]
Egg shell powder	Rhodamine B	1.99601	[36]
Egg shell powder	Congo red	1.22	[35]
Egg shell powder	Bromophenol blue	0.04	[35]
Egg shell powder	Malachite green	2.13	[35]
Egg shell powder	Murexide	1.03092	[36]
Egg shell powder	Eriochrome black T	1.56494	[36]
Egg shell powder	Reactive red 123 dye (RR123)	1.26	[37]
Egg shell membrane and egg shell powder	C.I. Reactive yellow 205, a sulphonated reactive azo dye,	48.78	[38]
Egg shell membrane and egg shell powder	Rhodamine B	0.72	[34]
Egg shell membrane	Rhodamine B	14.4	[34]
Egg shell powder/TiO ₂ (TiO ₂ /CES)	Acid red nylon 57 (AN57)	220.2	[39]
Egg shell powder/polymer mixture of alginate and polyvinyl alcohol (biocomposite adsorbent)	C.I. Remazol reactive red 198	46.9	[40]
Calcined eggshell powder/anthill clay composite	Methylene blue	43.46	[41]
CaO photocatalyst	Indigo carmine dye	~100% dye degradation (approx. 1 hr exposure)	[44]
CESP photocatalyst	Methylene blue	80% degradation (approx. 1 hr exposure)	This study

dye removal capacity considering egg shell powder, egg shell membrane, and mixture of both components. In addition, there are several composite materials developed utilizing egg shell powder. Table 3 provides a comparison of performance of egg shell powder in dye removal. In general, egg shell powder has a higher affinity for the anionic dyes compared to the cationic dyes. The MB adsorption on to CESP in this study is higher than the previously reported value for egg shell powders. Furthermore, recent studies on composite materials developed with egg shell powder indicate better removal capacity.

The photocatalytic ability of CaO was compared with TiO₂ by the work of Madhusudhana and coworkers for Violet GL2B azo dye and found that CaO is a more efficient catalyst compared to TiO₂ at high pH values. [55]. In another study, indigo carmine dye degradation was studied with CaO [44]. Table 3 provides a summary of utilizing egg shell-based materials for dye removal applications.

4. Conclusions

Egg shells are waste materials often without any reuse. Therefore, this study focused on how waste egg shell can be converted to a photocatalyst to remove toxic dye material. The two materials, raw egg shell powder (RESP) and calcined egg shell powder (CESP), have been compared for the dye removal efficiency under light and dark conditions. The enhanced dye degradation efficiency is observed with CESP in the presence of light compared to RESP suggesting it is a photocatalytic effect. The pseudo-second-order kinetic studies conducted for the RESP and CESP suggest MB is chemisorbed on the material. The equilibrium amount of dye adsorbed on the CESP is higher compared to RESP. The adsorption process best fitted with the Freundlich isotherm, suggesting monolayer of MB is adsorbed on to RESP and CESP. Furthermore, the CESP can be used to remove industrial dye Lanasy F5B with 1.17 mg/g equilibrium dye adsorption capacity. In conclusion, the CESP has enhanced performance for dye degradation compared to RESP, highlighting its potential use as a novel and eco-friendly photocatalyst for dye degradation.

Data Availability

Data relevant for XRD studies and efficiency calculation are included in the supporting information. If further data related to analysis are required, the corresponding author can provide upon request.

Conflicts of Interest

The authors declare that there are no conflicts of interest.

Acknowledgments

The authors thank Department Science and Technology; Department of Animal Science, Uva Wellassa University; and Instrument Center, Faculty of Applied Sciences, University of Sri Jayewardenepura, for providing facilities for this study. Dr. Thusitha Etampawala is acknowledged for the

discussions regarding XRD studies. The authors also thank Uva Wellassa University for the funding under grant UWU/R/G/2015/18.

Supplementary Materials

S1. Table 1: measurement conditions—raw egg shell powder (RESP). S1. Table 2: qualitative analysis results—raw egg shell powder and peak list (RESP). S1. Table 3: measurement conditions of calcined egg shell (CESP). S1. Table 4: qualitative analysis results of calcined egg shell and peak list (CESP). S2. Table 1: removal efficiency of RESP and CESP in dark condition. S2. Table 2: removal efficiency of RESP and CESP in light condition. S3. Figure 1: long exposure of MB on to the CESP in the light condition. S3. Figure 2: long exposure of MB on to CESP in dark condition. S3. Table 1: data of absorbance, equilibrium concentration, and equilibrium concentration of dye on the CESP and removal efficiency (dark). S3. Table 2: removal efficiency data of long exposure of MB with CESP powder (light). S4. Figure 1: adsorption isotherm trial for CESP. S5. Figure 1: UV-visible spectra of industrial dye. S5. Table 1: removal efficiency of industrial dye with CESP. S5. Figure 2: removal efficiency of industrial dye with CESP. (*Supplementary Materials*)

References

- [1] C. A. Gonzales, E. Riboli, and G. Lopez-Abente, "Bladder cancer among workers in the textile industry: results of a Spanish case-control study," *American Journal of Industrial Medicine*, vol. 14, no. 6, pp. 673–680, 1988.
- [2] Z. Singh and P. Chadha, "Textile industry and occupational cancer," *Journal of Occupational Medicine and Toxicology*, vol. 11, no. 1, p. 39, 2016.
- [3] T. Robinson, G. McMullan, R. Marchant, and P. Nigam, "Remediation of dyes in textile effluent: a critical review on current treatment technologies with a proposed alternative," *Bioresource Technology*, vol. 77, no. 3, pp. 247–255, 2001.
- [4] N. Kannan and M. M. Sundaram, "Kinetics and mechanism of removal of methylene blue by adsorption on various carbons—a comparative study," *Dyes and Pigments*, vol. 51, no. 1, pp. 25–40, 2001.
- [5] T. Robinson, B. Chandran, and P. Nigam, "Removal of dyes from a synthetic textile dye effluent by biosorption on apple pomace and wheat straw," *Water Research*, vol. 36, no. 11, pp. 2824–2830, 2002.
- [6] U. J. Etim, S. A. Umoren, and U. M. Eduok, "Coconut coir dust as a low cost adsorbent for the removal of cationic dye from aqueous solution," *Journal of Saudi Chemical Society*, vol. 20, pp. S67–S76, 2016.
- [7] A. M. Aljeboree, A. N. Alshirifi, and A. F. Alkaim, "Kinetics and equilibrium study for the adsorption of textile dyes on coconut shell activated carbon," *Arabian Journal of Chemistry*, vol. 10, pp. S3381–S3393, 2017.
- [8] M. W. Ashraf, N. Abulibdeh, and A. Salam, "Adsorption studies of textile dye (chrysoidine) from aqueous solutions using activated sawdust," *International Journal of Chemical Engineering*, vol. 2019, Article ID 9728156, 8 pages, 2019.
- [9] V. V. Pathak, R. Kothari, A. K. Chopra, and D. P. Singh, "Experimental and kinetic studies for phycoremediation and dye removal by *Chlorella pyrenoidosa* from textile wastewater,"

- Journal of Environmental Management*, vol. 163, pp. 270–277, 2015.
- [10] P. M. Dellamatrice, M. E. Silva-Stenico, L. A. B. de Moraes, M. F. Fiore, and R. T. R. Monteiro, "Degradation of textile dyes by cyanobacteria," *Brazilian Journal of Microbiology*, vol. 48, no. 1, pp. 25–31, 2017.
 - [11] C. A. Somensi, E. L. Simionatto, S. L. Bertoli, A. Wisniewski, and C. M. Radetski, "Use of ozone in a pilot-scale plant for textile wastewater pre-treatment: physico-chemical efficiency, degradation by-products identification and environmental toxicity of treated wastewater," *Journal of Hazardous Materials*, vol. 175, no. 1–3, pp. 235–240, 2010.
 - [12] A. Asghar, A. A. Abdul Raman, and W. M. Ashri Wan Daud, "Advanced oxidation processes for in-situ production of hydrogen peroxide/hydroxyl radical for textile wastewater treatment: a review," *Journal of Cleaner Production*, vol. 87, pp. 826–838, 2015.
 - [13] L. Bilińska, M. Gmurek, and S. Ledakowicz, "Comparison between industrial and simulated textile wastewater treatment by AOPs–biodegradability, toxicity and cost assessment," *Chemical Engineering Journal*, vol. 306, pp. 550–559, 2016.
 - [14] R. Liu, H. M. Chiu, R. Y.-L. Shiau, and Y.-T. Hung, "Degradation and sludge production of textile dyes by Fenton and photo-Fenton processes," *Dyes and Pigments*, vol. 73, no. 1, pp. 1–6, 2007.
 - [15] R. M. Reis, A. A. G. F. Beati, R. S. Rocha et al., "Use of gas diffusion electrode for the in situ generation of hydrogen peroxide in an electrochemical flow-by reactor," *Industrial & Engineering Chemistry Research*, vol. 51, no. 2, pp. 649–654, 2012.
 - [16] O. Carp, C. L. Huisman, and A. Reller, "Photoinduced reactivity of titanium dioxide," *Progress in Solid State Chemistry*, vol. 32, no. 1–2, pp. 33–177, 2004.
 - [17] U. G. Akpan and B. H. Hameed, "Parameters affecting the photocatalytic degradation of dyes using TiO₂-based photocatalysts: a review," *Journal of Hazardous Materials*, vol. 170, no. 2–3, pp. 520–529, 2009.
 - [18] A. J. Attia, S. H. Kadhim, and F. H. Hussein, "Photocatalytic degradation of textile dyeing wastewater using titanium dioxide and zinc oxide," *E-journal of Chemistry*, vol. 5, no. 2, pp. 219–223, 2008.
 - [19] N. Daneshvar, D. Salari, and A. R. Khataee, "Photocatalytic degradation of azo dye acid red 14 in water on ZnO as an alternative catalyst to TiO₂," *Journal of Photochemistry and Photobiology A: Chemistry*, vol. 162, no. 2–3, pp. 317–322, 2004.
 - [20] J. Nishio, M. Tokumura, H. T. Znad, and Y. Kawase, "Photocatalytic decolorization of azo-dye with zinc oxide powder in an external UV light irradiation slurry photoreactor," *Journal of Hazardous Materials*, vol. 138, no. 1, pp. 106–115, 2006.
 - [21] T. Le Thi Thanh, L. Nguyen Thi, T. T. Dinh, and N. Nguyen Van, "Enhanced photocatalytic degradation of Rhodamine B using C/Fe Co-doped titanium dioxide coated on activated carbon," *Journal of Chemistry*, vol. 2019, Article ID 2949316, 8 pages, 2019.
 - [22] S. Kansal, M. Singh, and D. Sud, "Studies on photo-degradation of two commercial dyes in aqueous phase using different photocatalysts," *Journal of Hazardous Materials*, vol. 141, no. 3, pp. 581–590, 2007.
 - [23] A. Ajmal, I. Majeed, R. N. Malik et al., "Photocatalytic degradation of textile dyes on Cu₂O-CuO/TiO₂ anatase powders," *Journal of Environmental Chemical Engineering*, vol. 4, no. 2, pp. 2138–2146, 2016.
 - [24] R. Saravanan, M. Mansoob Khan, V. K. Gupta et al., "ZnO/Ag/CdO nanocomposite for visible light-induced photocatalytic degradation of industrial textile effluents," *Journal of Colloid and Interface Science*, vol. 452, pp. 126–133, 2015.
 - [25] R. Saravanan, E. Sacari, F. Gracia, M. M. Khan, E. Mosquera, and V. K. Gupta, "Conducting PANI stimulated ZnO system for visible light photocatalytic degradation of coloured dyes," *Journal of Molecular Liquids*, vol. 221, pp. 1029–1033, 2016.
 - [26] C. Piccirillo and P. M. L. Castro, "Calcium hydroxyapatite-based photocatalysts for environment remediation: characteristics, performances and future perspectives," *Journal of Environmental Management*, vol. 193, pp. 79–91, 2017.
 - [27] M. Sun, D. Li, Y. Chen et al., "Synthesis and photocatalytic activity of calcium antimony oxide hydroxide for the degradation of dyes in water," *The Journal of Physical Chemistry C*, vol. 113, no. 31, pp. 13825–13831, 2009.
 - [28] M. Kouzu, T. Kasuno, M. Tajika, Y. Sugimoto, S. Yamanaka, and J. Hidaka, "Calcium oxide as a solid base catalyst for transesterification of soybean oil and its application to biodiesel production," *Fuel*, vol. 87, no. 12, pp. 2798–2806, 2008.
 - [29] <https://www.wattagnet.com/articles/36268-latest-poultry-egg-market-forecasts-available-in-2018-watt-poultry-trends>.
 - [30] F. Hamideh and A. Akbar, "Application of eggshell wastes as valuable and utilizable products: a review," *Research in Agricultural Engineering*, vol. 64, no. 2, pp. 104–114, 2018.
 - [31] A. Mittal, M. Teotia, R. K. Soni, and J. Mittal, "Applications of egg shell and egg shell membrane as adsorbents: a review," *Journal of Molecular Liquids*, vol. 223, pp. 376–387, 2016.
 - [32] W.-T. Tsai, K.-J. Hsien, H.-C. Hsu, C.-M. Lin, K.-Y. Lin, and C.-H. Chiu, "Utilization of ground eggshell waste as an adsorbent for the removal of dyes from aqueous solution," *Bioresource Technology*, vol. 99, no. 6, pp. 1623–1629, 2008.
 - [33] M. A. Zulfikar, A. W. Mohammad, and S. Henry, "Adsorption of congo red from aqueous solution using powdered eggshell," *International Journal of Chemtech Research*, vol. 5, no. 4, pp. 1532–1540, 2013.
 - [34] W. Bessashia, Z. Hattab, Y. Berredjem et al., "Utilization of powdered eggshell waste for rhodamine B removal: evaluation of adsorptive efficiencies and modeling studies," *Sensor Letters*, vol. 16, no. 2, pp. 128–136, 2018.
 - [35] E. Rápó, R. Szép, A. Keresztesi, M. Suciú, and S. Tonk, "Adsorptive removal of cationic and anionic dyes from aqueous solutions by using eggshell household waste as biosorbent," *Acta Chimica Slovenica*, vol. 65, no. 3, pp. 709–717, 2018.
 - [36] A. V. Borhade and A. S. Kale, "Calcined eggshell as a cost effective material for removal of dyes from aqueous solution," *Applied Water Science*, vol. 7, no. 8, pp. 4255–4268, 2017.
 - [37] M. Ehrampoush, G. H. Ghanizadeh, and M. Ghaneian, "Equilibrium and kinetics study of reactive red 123 dye removal from aqueous solution by adsorption on eggshell," *Journal of Environmental Health Science & Engineering*, vol. 8, no. 2, pp. 101–106, 2011.
 - [38] N. Pramanpol and N. Nitayapat, "Adsorption of reactive dye by eggshell and its membrane," *Kasetsart Journal: Natural Science*, vol. 40, pp. 192–197, 2006.
 - [39] M. A. El-Kemary, I. M. El-mehasseb, and K. R. Shoueir, "Sol-gel TiO₂ decorated on eggshell nanocrystal as engineered adsorbents for removal of acid dye," *Journal of Dispersion Science and Technology*, vol. 39, no. 6, pp. 911–921, 2018.
 - [40] M. F. Elkady, A. M. Ibrahim, and M. M. A. El-Latif, "Assessment of the adsorption kinetics, equilibrium and thermodynamic for the potential removal of reactive red dye using

- eggshell biocomposite beads,” *Desalination*, vol. 278, no. 1–3, pp. 412–423, 2011.
- [41] A. S. Yusuff, “Adsorption of cationic dye from aqueous solution using composite chicken eggshell-anthill clay: optimization of adsorbent preparation conditions,” *Acta Polytechnica*, vol. 59, no. 2, pp. 192–202, 2019.
- [42] M. N. Zafar, M. Amjad, M. Tabassum, I. Ahmad, M. Zubair, and M. Zubair, “SrFe₂O₄ nanoferrites and SrFe₂O₄/ground eggshell nanocomposites: fast and efficient adsorbents for dyes removal,” *Journal of Cleaner Production*, vol. 199, pp. 983–994, 2018.
- [43] <https://www.britannica.com/technology/calcination>.
- [44] K. D. Veeranna, M. T. Lakshamaiah, and R. T. Narayan, “Photocatalytic degradation of indigo carmine dye using calcium oxide,” *International Journal of Photochemistry*, vol. 2014, Article ID 530570, 6 pages, 2014.
- [45] W. T. Tsai, J. M. Yang, C. W. Lai, Y. H. Cheng, C. C. Lin, and C. W. Yeh, “Characterization and adsorption properties of eggshells and eggshell membrane,” *Bioresource Technology*, vol. 97, no. 3, pp. 488–493, 2006.
- [46] M. El Haddad, A. Regti, M. R. Laamari et al., “Calcined mussel shells as a new and eco-friendly biosorbent to remove textile dyes from aqueous solutions,” *Journal of the Taiwan Institute of Chemical Engineers*, vol. 45, no. 2, pp. 533–540, 2014.
- [47] D. Yang, T. Fan, Z. Han, J. Ding, and D. Zhang, “Biogenic hierarchical TiO₂/SiO₂ derived from rice husk and enhanced photocatalytic properties for dye degradation,” *PLoS One*, vol. 6, no. 9, Article ID e24788, 2011.
- [48] A. Houas, H. Lachheb, M. Ksibi, E. Elaloui, C. Guillard, and J.-M. Herrmann, “Photocatalytic degradation pathway of methylene blue in water,” *Applied Catalysis B: Environmental*, vol. 31, no. 2, pp. 145–157, 2001.
- [49] S. Zhang, “A new nano-sized calcium hydroxide photocatalytic material for the photodegradation of organic dyes,” *RSC Advances*, vol. 4, no. 31, pp. 15835–15840, 2014.
- [50] F. M. Hossain, G. E. Murch, I. V. Belova, and B. D. Turner, “Electronic, optical and bonding properties of CaCO₃ calcite,” *Solid State Communications*, vol. 149, no. 29–30, pp. 1201–1203, 2009.
- [51] R. Zuo, G. Du, W. Zhang et al., “Photocatalytic degradation of methylene blue using TiO₂ impregnated diatomite,” *Advances in Materials Science and Engineering*, vol. 2014, Article ID 170148, 7 pages, 2014.
- [52] C. An, S. Peng, and Y. Sun, “Facile synthesis of sunlight-driven AgCl:Ag plasmonic nanophotocatalyst,” *Advanced Materials*, vol. 22, no. 23, pp. 2570–2574, 2010.
- [53] S. Karagoz, T. Tay, and M. Erdem, “Activated carbons from waste biomass by sulfuric acid activation and their use on methylene blue adsorption,” *Bioresource Technology*, vol. 99, no. 14, pp. 6214–6222, 2008.
- [54] Y. S. Ho and G. McKay, “Pseudo-second order model for sorption processes,” *Process Biochemistry*, vol. 34, no. 5, pp. 451–465, 1999.
- [55] N. Madhusudhana, K. Yogendra, and K. M. Mahadevan, “A comparative study on Photocatalytic degradation of Violet GL2B azo dye using CaO and TiO₂ nanoparticles,” *International Journal of Engineering Research and Applications*, vol. 2, no. 5, pp. 1300–1307, 2012.

Research Article

Preparation, Characterization, and Application of Metakaolin-Based Geopolymer for Removal of Methylene Blue from Aqueous Solution

Marouane El Alouani , Saliha Alehyen, Mohammed El Achouri, and M'hamed Taibi

Mohammed V University in Rabat, Laboratoire de Physico-chimie des Matériaux Inorganiques et Organiques (LPCMIO), Ecole Normale Supérieure (ENS), Centre des Sciences des Matériaux (CSM), Rabat, Morocco

Correspondence should be addressed to Marouane El Alouani; ma.elalouani@gmail.com

Received 30 January 2019; Revised 5 April 2019; Accepted 14 April 2019; Published 28 May 2019

Guest Editor: Mohamed Zbair

Copyright © 2019 Marouane El Alouani et al. This is an open access article distributed under the Creative Commons Attribution License, which permits unrestricted use, distribution, and reproduction in any medium, provided the original work is properly cited.

Metakaolin-based geopolymers are aluminosilicate materials that can be used as cationic dye adsorbents in aqueous system treatment. Our aim in this paper is to study the ability of geopolymer powder produced from metakaolin and alkaline activators to act as an adsorbent to remove methylene blue (MB). The solid materials were systematically analyzed by X-ray fluorescence (XRF), X-ray diffraction (XRD), Fourier-transform infrared spectrometry (FTIR), scanning electron microscopy (SEM), energy dispersive X-ray analysis (EDX), and the point of zero charge. XRF, FTIR, XRD, SEM, and EDX analyses confirmed the formation of a geopolymer composite by geopolymerization reaction. The influence of various experimental factors such as geopolymer dosage, pH, initial dye concentration, contact time, and temperature was assessed. Adsorption isotherms were evaluated by Langmuir, Freundlich, Temkin, and Dubinin–Radushkevich isotherms. Kinetics data were studied using pseudo-first-order, pseudo-second-order, and intraparticle diffusion models. The thermodynamic parameters, namely, Gibbs free energy (ΔG°), enthalpy (ΔH°), and entropy (ΔS°), were determined. The results indicated that the maximum decolorization was found in high pH values. The collected isotherm data were best fitted by the Langmuir isotherm, and the maximum adsorption capacity of dye onto the geopolymer was 43.48 mg/g. The experiment kinetics followed the pseudo-second-order kinetic models. The thermodynamic results demonstrated that the adsorption of the obtained material occurs spontaneously as an endothermic process. The results confirmed that the prepared adsorbent can be used for remediation of water contaminated by MB dye.

1. Introduction

The rapid industrial growth has led to the release of different dyes in the aquatic environment, and the treatment of effluents has become a challenging topic in environmental sciences. With the wide applications of dyes in multiple fields such as textile, leather, additives, petroleum product, paper, cotton, wool, plastic, and pharmaceutical industries, water pollution caused by the colorants is increased, which has attracted the attention of the scientific community [1, 2]. Generally, synthetic nondegradable dyes not only pollute water resources but also affect the human health because of their toxic nature [3]. In addition, their presence in aquatic systems, even at low concentrations, reduces the penetration of light and therefore has a detrimental effect on photosynthesis [4]. Consequently,

the presence of trace amounts of these micropollutants (<1 ppm) in industrial wastewater is extremely noticeable and unwanted [5]. Among the most used industrial dyes, methylene blue (MB) is a basic dyestuff widely used in various industries such as textile dyeing, petroleum industries, and color photography. Therefore, the treatment of water contaminated by these chemicals is necessary both for the protection of the environment and for the reuse of these unconventional waters. In recent years, different techniques have been developed and tested to recover toxic substances from wastewaters before discharging into an aquatic environment, such as coagulation [6], advanced oxidation [7], photocatalytic degradation [8], ultrafiltration [9], ion-exchange [10], electrochemical treatment [11], and adsorption [12–15]. Among various physicochemical processes,

adsorption is a technique of choice due to its low cost, simple design, and reusability [16, 17]. Different categories of natural and synthetic adsorbents were utilized for the removal of this organic material from aquatic media, such as kaolin [18], zeolite [19], activated carbon [20], mesoporous birnessite [1], natural clay [21], magnetic chitosan [22], fruit peels [23], biochar microparticles [24], silica [25], loofah sponge-based porous carbons [26], pyrophyllite [24], and Fe₃O₄/activated montmorillonite nanocomposite [27]. Among the synthesized adsorbents mostly used to remove organic matters are geopolymers [28]. Geopolymers, firstly named by Joseph Davidovits [29], are formed by activation of aluminosilicate precursors, and these solids can be natural (kaolin, mica, andalusite, spinelle, illite, or Slag Hill) or synthetic (metakaolin, fly ash, calcined by-products, or industrial residues) activated by alkali silicate solution (typically Na or K) at temperatures between 20°C and 100°C [30]. Corresponding to different Si/Al ratios, the materials are composed of network structures of (Na, K)-poly(sialate) (-O-Si-O-Al-O-)_n, (Na, K)-poly(sialat-siloxo) (-O-Si-O-Al-O-Si-O-)_n, and (Na, K)-poly(sialate-disiloxo) (O-Si-O-Al-O-Si-O-Si-O-)_n [29]. The geopolymers or inorganic polymers have also gained significant attention as efficient adsorbents with good physical and chemical properties. Recently, several studies were conducted in the interest of activation of aluminosilicate precursors characterized and tested for removal of dyestuffs and hazardous materials from aquatic environment [8, 31, 32].

In this work, a geopolymerization method was applied to synthesize the metakaolin-based geopolymer. The structural and morphological properties of the elaborated adsorbent were characterized by XRF, XRD, FTIR, and SEM analyses. The adsorption properties of the elaborated sample were studied in different experimental conditions, including adsorbent mass, pH, contact time, initial dye solution, and temperature. The adsorption kinetics, isotherms, and thermodynamics data of the adsorption were investigated to study the batch adsorption process of the basic dye using the synthesized metakaolin-based geopolymer.

2. Materials and Experimental Methods

2.1. Materials and Chemicals. Kaolin was collected from Bab Mssila situated at Ribat El Kheir next to Sefrou city in the northwest of Morocco. The raw clay was subjected to calcination at temperatures of 800°C for 3 h.

The industrial-grade sodium silicate powder (Honeywell Riedel-de Haën, Germany; 18 wt.% Na₂O, 63 wt.% SiO₂, 18 wt.% loss on ignition) and commercial sodium hydroxide (NaOH; 99% purity) (ACS AR-grade pellets) were provided by Sigma-Aldrich. Methylene blue (MB) dye with the chemical composition C₁₆H₁₈ClN₃S and a MW of 319,852 g/mol was supplied by Sigma-Aldrich.

2.2. Geopolymer Synthesis. The geopolymer sample was synthesized in several steps. The first step was to synthesize the activator solution by initially dissolving Na₂SiO₃ powder and sodium hydroxide NaOH (12 M) at a mass ratio of 2.5 [33]. The mixture was stirred at room temperature for a

period of 15 min. The second step of the elaboration is the mixing of metakaolin with the activator solution, which was conducted using in a mixer with constant stirring at ambient temperature for 15 min to obtain good homogenization. Then, distilled water was added at a ratio water/metakaolin of 0.34 to obtain the desired workability of the geopolymer paste. The mixture was placed in a cylindrical mould and treated at 60°C for 24 hours. Finally, the matrix was sieved to particle sizes <200 μm and stored in a desiccator for characterization and investigation of the adsorption tests. The mix proportions of the metakaolin-based geopolymer pastes are displayed in Table 1.

2.3. Adsorption Experiments. A series of batch adsorption experiments were carried out under different operating conditions related to adsorbent mass (0.05–0.35 g), contact time (0–220 min), initial solution pH (2–13), initial dye concentration (5–60 mg/L), and temperature (20–70°C), at a constant agitation speed (250 rpm) (Table 2). The solution pH was adjusted to optimum values using 0.1 M NaOH or 0.1 M HCl. Afterwards, the sample was centrifuged at 2500 rpm for 10 min. The initial and the residual concentrations of MB were measured using a spectrophotometer at a wavelength of 664 nm. The removal efficiency of the metakaolin-based geopolymer was calculated using equation (1), adsorption capacity at any time q_t (mg·g⁻¹) was obtained using equation (2), and adsorption capacity at equilibrium q_e (mg·g⁻¹) was determined using equation (3):

$$\% \text{ removal} = \frac{(C_i - C_t)}{C_i} \times 100, \quad (1)$$

$$q_t = \frac{(C_i - C_t)}{m} V, \quad (2)$$

$$q_e = \frac{(C_i - C_e)}{m} V, \quad (3)$$

where C_i (mg·L⁻¹) is the initial concentration of MB solution, C_e (mg·L⁻¹) and C_t (mg·L⁻¹) are, respectively, the liquid-phase concentration of MB at initial time and at any time t after the adsorption process, m (g) is the weight of geopolymer, and V (L) is the volume of the MB solution.

2.4. Instrument Analysis. The chemical compositions of materials and the prepared adsorbent were determined by X-ray fluorescence using a spectrometer dispersion wavelength-type Axios. The crystalline phases of the sample were detected using an X-ray diffractometer (Philips model 1840 equipment). The functional groups of samples were detected using Fourier-transform infrared spectrometry bruker platinum ATR apparatus, in the range of 4000–400 cm⁻¹ wavelengths. The microstructure of metakaolin and metakaolin-based geopolymer was observed using the JEOL-6300F field-scanning electron microscope (SEM/EDX). The concentration of MB was determined using the spectrophotometer JASCO V-630 UV/VIS. A pH-meter model (M 210) was used for pH measurement.

TABLE 1: Chemical formulation of geopolymer.

Mixture of geopolymer	Metakaolin (g)	NaOH (g)	Silicate (g)	Mass of water of NaOH dilution (g)	Extra water (g)	Total water (g)	Ratio water/metakaolin	Ratio metakaolin/alkaline activator	Ratio $\text{Na}_2\text{SiO}_3/\text{NaOH}$
Mass ratio (g)	50	5.715	14.285	11.905	5	16.905	0.34	2.5	2.5

TABLE 2: Experimental conditions for the adsorption of MB on geopolymer.

Investigated parameter	Temperature ($^{\circ}\text{C}$)	pH	Geopolymer dosage (g)	Contact time (min)	Initial concentration (mg/L)
Geopolymer dosage (g)	25	5	0.05	120	40
			0.1		
			0.15		
			0.2		
			0.25		
			0.3		
			0.35		
Contact time (min)	25	5	0.1	0	20, 30, 40
				30	
				60	
				90	
				120	
				150	
				180	
220					
pH	25	2.21	0.1	120	40
		4.46			
		6.16			
		8.09			
		10.06			
12.06					
Temperature ($^{\circ}\text{C}$)	20	5	0.1	120	40
	50				
	70				
Initial concentration (mg/L)	25	5	0.1	120	5
					10
					20
					40
					60

The pH at the point of zero charge (pH_{pzc}) of the geopolymer was determined by the method described by Pawar et al. [34]. A series of (0.01 M) KNO_3 solution ($V = 100$ mL) were prepared, and the initial pH of KNO_3 was adjusted to a given value from pH 2 to 13 by the addition of HCl (0.1 M) or NaOH (0.1 M). To each solution, 0.1 g of geopolymer was added and shaken for 48 h with an agitation speed of 120 rpm at room temperature. The differences between the pH value of the initial solution (pH_i) and the final solution (pH_f) were plotted as a function of pH_i . The point of intersection of this curve yielded the point of zero charge.

3. Results and Discussion

3.1. Structural Analysis

3.1.1. Chemical Analysis of Solids. The chemical composition of metakaolin and the synthesized sample is illustrated in

Table 3. The XRF analysis indicates that the metakaolin is basically formed by SiO_2 , Al_2O_3 , and Na_2O . After activation of metakaolin by the alkali solution, it was found that a new inorganic material with an Si/Al ratio of approximately 2.04 was formed, indicating the poly(sialate-siloxo) (PSS) ($-\text{Si}-\text{O}-\text{Al}-\text{O}-\text{Si}-\text{O}-$) $_n$ nature of the formed material [35].

3.1.2. X-Ray Diffraction. Figure 1 shows the XRD patterns of kaolin, metakaolin, and geopolymer. The results of DRX analysis for kaolin show that the material is rich in kaolinite and quartz. After calcination, the disappearance of the peaks corresponding to kaolinite is observed, which is explained by the dehydroxylation of the water molecules that exist in the kaolinite structure in metakaolinite by heat treatment [36]. After the activation process, the crystalline phases were dissolved in the alkaline solution and the aluminosilicate phase was formed in the surface of metakaolin by geopolymerization reaction [37]. These results indicated the

TABLE 3: Quantitative chemical composition of metakaolin and geopolymer.

Oxides (wt.%)	Metakaolin	Geopolymer	Elements (wt.%)	Metakaolin	Geopolymer
SiO ₂	37.6	31	O	46.7	45.6
Al ₂ O ₃	19.6	13.4	Na	11	20.4
Na ₂ O	14.9	27.5	Si	17.6	14.5
MgO	8.46	5.94	Al	10.4	7.08
CaO	2.35	1.66	Fe	1.92	1.29
Fe ₂ O ₃	2.75	1.85	K	1.32	0.936
K ₂ O	1.5	1.13	Ca	1.68	1.19
SO ₃	4.14	3.4	S	1.66	1.36
Loss on ignition	7.74	13.5	Mg	5.4	3.58
SiO ₃ /Al ₂ O ₃	1.92	2.31	Si/Al	1.7	2.04

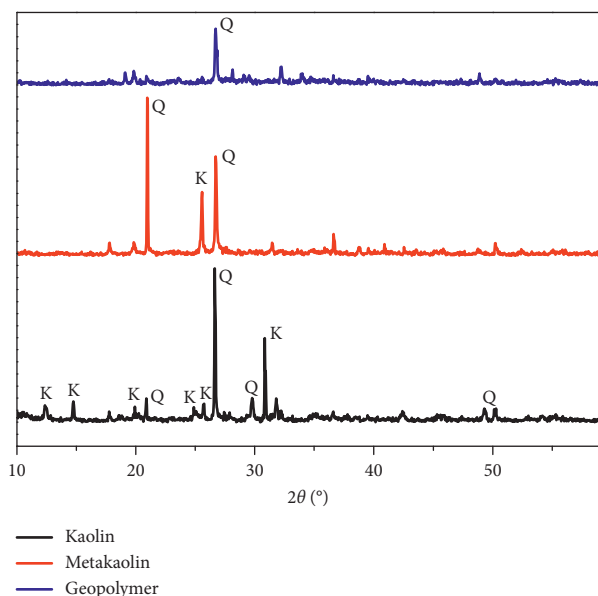


FIGURE 1: XRD patterns of kaolin, metakaolin, and geopolymer.

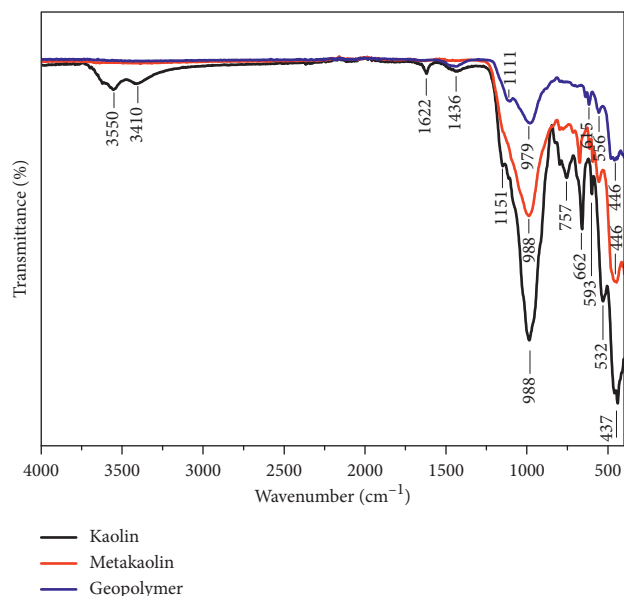


FIGURE 2: FTIR spectrum of kaolin, metakaolin, and geopolymer.

formation of a new product with a structure different from that of metakaolin.

3.1.3. Infrared Spectroscopy. The FTIR spectra of kaolin, metakaolin, and elaborated matrix are depicted in Figure 2, and all the band assignments are presented in Table 4. In kaolin, the bands at 3350 and 1622 cm⁻¹ correspond to OH stretching and deformation of the hydroxyl group, respectively. The adsorption band appearing at 1436 cm⁻¹ is related to the stretching vibrations of O-C-O due to atmospheric carbonation on the surface of kaolin. The band at 1151 cm⁻¹ is due to the Si-O outside of the plane-stretching vibration. The most intensive band at 998 was due to Si-O-Al stretching vibration. Bands which exist between 757 cm⁻¹ and 532 cm⁻¹ correspond to stretching vibrations of Si-O-Al. The band at 437 cm⁻¹ is related to the Si-O-Si bending vibration. After calcination, no bands were observed between 3350 and 1622 cm⁻¹ in metakaolin, suggesting that the thermal treatment was adequate to convert kaolin to metakaolin. The asymmetric stretching vibration of Si-O-T (T=Al or Si) at 988 cm⁻¹ in metakaolin shifted

approximately 9 cm⁻¹ after the geopolymerization reaction to 979 cm⁻¹. The shifting and reduction of peaks in FTIR spectrum confirms the formation of a the poly(sialate-siloxo) chain in the structure by geopolymerization reaction [47].

3.1.4. Microstructural Analysis (SEM/EDX). Figure 3 shows the representative SEM images of metakaolin and the synthesized matrix. The surface morphology of metakaolin was different from that of the geopolymer matrix. SEM images (Figure 3(a)) of metakaolin showed that the sample is a heterogeneous material consisting of irregularly shaped particles. After the geopolymerization reaction (Figure 3(b)), the morphology of the geopolymer is constituted by a chain of polysilicate layers by the complete disappearance of metakaolin particles. This morphological change observed in the synthesized geopolymer is due to the dissolution of metakaolin aluminosilicates in the activator solution leading to the formation of aluminosilicate gel. EDX microanalysis was used to characterize the elemental composition of the metakaolin and geopolymer (Figure 3). According to the

TABLE 4: FTIR bands (cm^{-1}) of kaolin, metakaolin, and geopolymer.

Kaolin	Bands (cm^{-1})		Assignments	References
	Metakaolin	Geopolymer		
3550	—	—	Stretching and deformation of OH	[38]
3410	—	—	Stretching and deformation of OH	[34]
1622	—	—	Stretching and deformation of OH	[34]
1436	—	—	Stretching vibration of O-C-O	[39]
1151	—	1111	Si-O-Si bending vibration	[40]
988	988	979	Stretching vibration of Si-O-T (T = Al or si)	[41]
757	757	—	Bending vibration of Si-O-Al	[42]
662	662	664	Bending vibration of Si-O-Al	[43]
593	593	—	Bending vibration of Si-O-Al	[44]
532	553	553	Bending vibration of Si-O-Al	[45]
437	446	446	Bending vibration of Si-O-Si	[46]

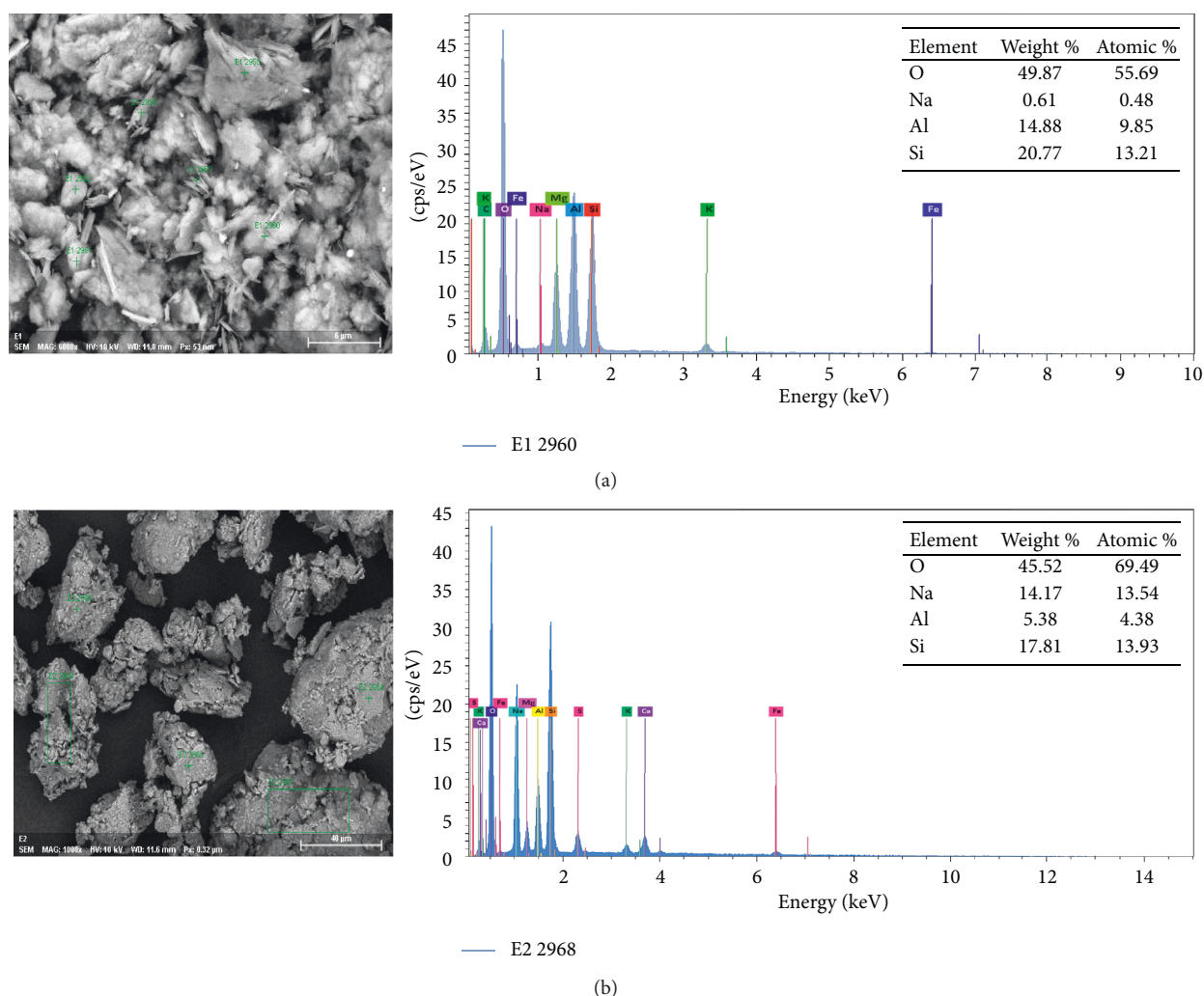


FIGURE 3: SEM micrographs and energy dispersive X-ray analysis (EDX) of metakaolin (a) and geopolymer (b).

EDX analysis (Figure 3(a)), the major elements were oxygen, silicon, and aluminum, with proportion values of 49.87, 20.77, and 14.88%, respectively. The percentage of sodium elements increased from 0.61 to 14.17% (Figure 3(b)); this is due to the alkali activator used in the geopolymerization process.

3.2. Batch Adsorption Test

3.2.1. Effect of Adsorbent Dose. The effect of adsorbent dose on the removal of MB was investigated, and the results are shown in Figure 4. As can be seen, when the geopolymer mass increased from 0.05 to 0.35 g/L, the MB removal

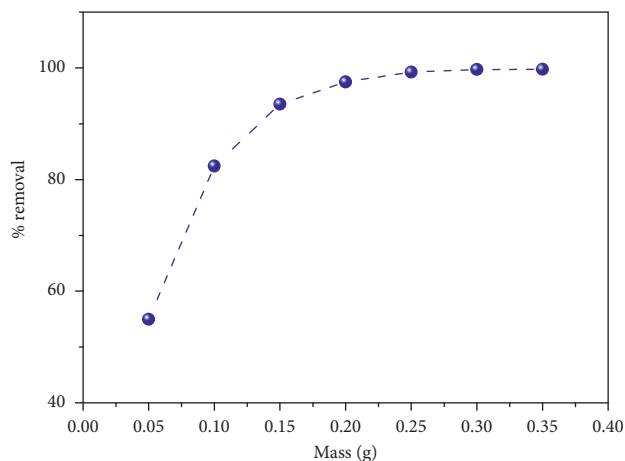


FIGURE 4: Effect of adsorbent dose on the removal efficiency.

efficiency increased from 55% to 99.77%. This result might attribute to the increasing number of binding sites in the geopolymer for MB removal by increasing the quantity of adsorbents [48]. A similar trend was obtained for this toxic dye removal on the geopolymer paste [49] and phosphoric acid-based geopolymers [50]. Optimizing the mass of the adsorbent is a very important parameter for controlling the adsorption capacity. According to the experimental results, the adsorption assays should be performed using 0.1 g/100 mL for MB.

3.2.2. Effect of pH on the Removal Efficiency and pH Point of Zero Charge (pH_{pzc}) of Geopolymer. The influence of pH is an important factor for removal of organic matter from water. Figure 5(a) represents the effect of the solution's initial pH in the adsorption process. It is observed that the removal efficiency increases with the rise in the pH value and reaches 91.2% at a pH value of 12.06. The removal is affected by the change in the pH value of the solution. In acidic medium, the surface of the geopolymer is surrounded by H^+ ions, which decrease the interaction of the solute ions (MB^+) with the sites of the geopolymeric material. On the contrary, in the basic medium, the concentration of H^+ ions decreases and generates a good interaction between the dye ions and the sites of the surface. Similar adsorption behaviors of MB were reported by several investigations [20, 51]. In order to confirm this result, it is necessary to determine the pH_{pzc} of the adsorbent. The zero point of charge (PZC) is defined as the number of positive charges equal to the number of negative charges that exist on the surface of the adsorbent. The pH_{pzc} of the geopolymer is shown in Figure 5(b) and the pH_{pzc} value of the adsorbent was found almost to be 9. Thus, at $pH < 9$, the surface of the geopolymer is positively charged and becomes negatively charged at $pH > 9$. Therefore, with increasing pH above $pH_{pzc} = 9$, the removal of cationic dye by the geopolymer increased slightly. The removal increase can be explained by electrostatic attraction between the particles of the geopolymer, which is negatively charged, and the cationic dye, which is positively charged [52]. These results show that the attraction between the

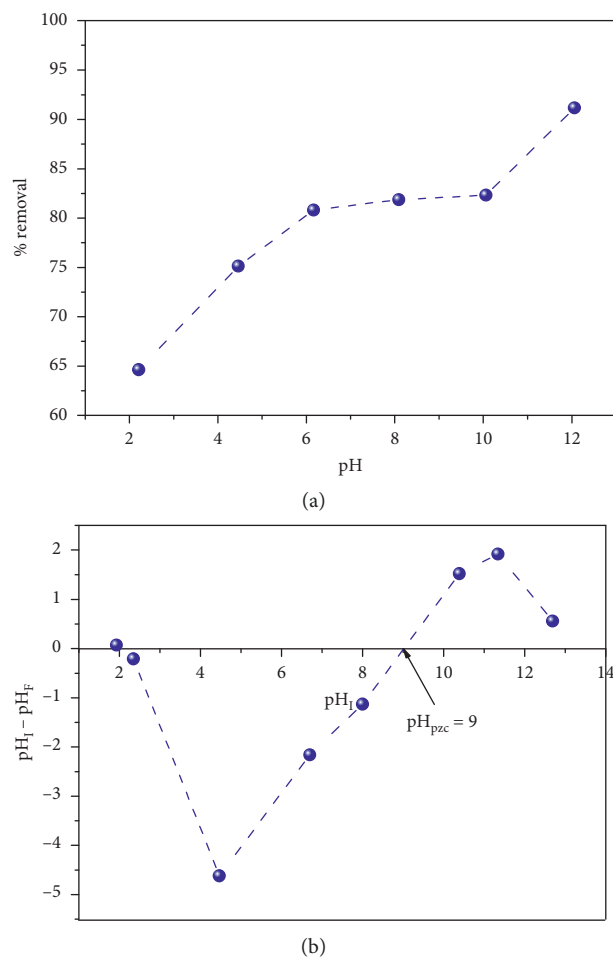


FIGURE 5: Effect of pH on adsorption of MB onto geopolymer (a) and point of zero charge (pH_{pzc}) of geopolymer (b).

inorganic framework (negatively charged) and the methylene blue (positively charged) depends on pH.

3.2.3. Effect of Contact Time and Kinetics

(1) Effect of Contact Time. The effect of contact time on the removal of MB by the geopolymer is shown in Figure 6. The results demonstrate that the removal percentage of MB is rapid in the first 30 min of contact time. Afterwards, the equilibrium time is reached within 180, 180, and 150 min for 20, 30, and 40 mg/L, respectively. After the equilibrium, no significant change in the removal percentage of the geopolymer was observed in the different dye concentration. It was observed that for an increased contact time from 30 to 240 min, the efficiency augmented from 87.50 to 100%, 90 to 99%, and 87.50 to 97.90% for concentrations of 20, 30, and 40 mg/L, respectively. It can be seen that the decrease of MB removal with increasing initial MB concentration is due to the saturation of the adsorbent surface at high dye concentrations. Similar result was reported by Hamid et al. [53].

(2) Kinetics Studies. There are several mathematical models used to describe the adsorption kinetics of pollutants onto the adsorbent material. In this study, three kinetic models

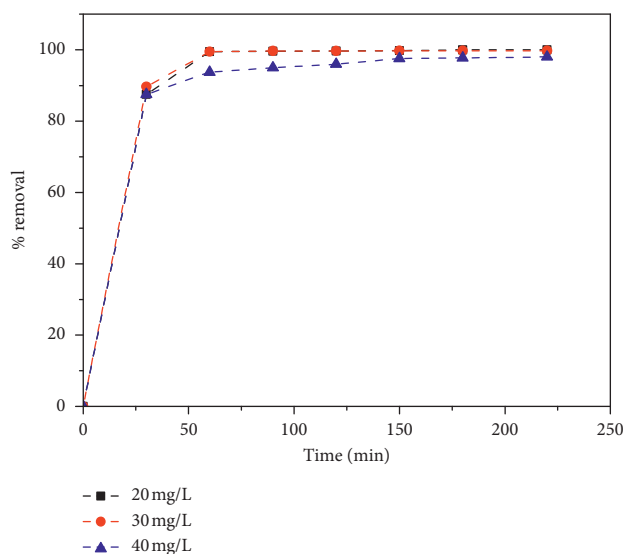


FIGURE 6: Effect of contact time on adsorption of MB onto geopolymer.

(pseudo-first-order, pseudo-second-order, and intraparticle diffusion) were applied for the adsorption of MB by the geopolymer to describe the adsorption process.

The pseudo-first-order model [54] is expressed as follows:

$$\ln(q_e - q_t) = \ln q_e - k_1 t. \quad (4)$$

The pseudo-second-order model [55] is represented by the following equation:

$$\frac{t}{q_t} = \frac{1}{k_2 q_e^2} + \frac{t}{q_e}. \quad (5)$$

The intraparticle diffusion model [56] is given by the following equation:

$$q_t = k_1 t^{1/2} + I, \quad (6)$$

where q_e (mg/g) is the adsorption capacity at equilibrium, q_t (mg/g) is the adsorbed concentration of MB at time t , k_1 (1/min) is the pseudo-first-order rate constant for the adsorption process, k_2 (g/mg·min) is the pseudo-second-order rate constant for the adsorption process, k_1 (mg/(g·min^{0.5})) is the intraparticle diffusion rate constant, and I (mg/g) is the intercept.

The fitting results are shown in Figures 7(a)–7(c), and the kinetics constants and correlation coefficients calculated for pseudo-first-order, pseudo-second-order, and intraparticle-diffusion equations are listed in Table 5. These results revealed that the adsorption of MB on the geopolymer matrix is best described by the pseudo-second-order kinetic model with a high correlation coefficient (0.999), and the calculated $q_{e(\text{cal})}$ values are in agreement with experimental $q_{e(\text{exp})}$ values at different initial MB concentrations. These results indicate that the chemical interaction process involves electron sharing and exchange between MB and functional groups of the geopolymer [57]. Similar results were also found in previous studies [23, 58].

The silicate geopolymer network consists of (SiO₄) and (AlO₄) groups connected by covalent bond Si-O-Al-. The (Na⁺) cations present in the structural cavities of the poly(sialate) balance the negative charge of Al³⁺ in coordination (IV) [29]. During the adsorption phenomena, the removal of MB by the adsorbent can be explained by the interactions between the positive charge of (MB⁺) and the negative charge of Al tetrahedral (-Si-O-Al⁻-O-Si-O) in the metakaolin-based geopolymer (Figure 8). This proposed mechanism explains the chemisorption of methylene blue by the metakaolin-based geopolymer.

3.2.4. Effect of Initial Concentration Dye and Isotherms

(1) *Effect of Initial Concentration Dye.* The effect of varying MB initial concentration on the adsorption capacity of MB by the geopolymer is shown in Figure 9. It can be seen that the adsorption capacity of MB increased as the initial MB concentration increased. Adsorption capacities of the geopolymer increase with the initial MB concentration increase due to the increase in the driving force of the concentration gradient [59]. A similar observation was reported previously for MB removal on mesoporous birnessite [1] and Cu-BTC [58].

(2) *Isotherm Studies.* To investigate the adsorption mechanism of the distribution of adsorbate molecules between the liquid and the solid phase, four different models (Langmuir, Freundlich, Temkin, and Dubinin–Radushkevich) were employed to fit the adsorption data.

3.3. *Langmuir Isotherm.* Langmuir isotherm model is applied to explain the adsorption mechanism onto a homogeneous surface and calculate the monolayer adsorption capacity in the surface of the adsorbent [60]. This model is expressed by the following:

$$\frac{C_e}{q_e} = \frac{1}{K_L q_m} + \frac{C_e}{q_m}, \quad (7)$$

where q_e is the amount of dye at equilibrium (mg/g), C_e is the equilibrium concentration of the pollutant (mg/L), q_m is the amount of monolayer adsorption capacity (mg/g), and K_L is the Langmuir constant (L/mg).

The essential characteristic of the Langmuir isotherm can be expressed by the dimensionless constant separation factor R_L defined by following relationship:

$$R_L = \frac{1}{1 + K_L C_0}, \quad (8)$$

where K_L (L/mg) is the Langmuir adsorption constant, C_0 (mg/L) is the initial MB concentration. The R_L values classification is given in Table 6 [61].

3.4. *Freundlich Isotherm.* The Freundlich model is applicable to describe the multilayer adsorption process on active sites [62].

A linear form of the Freundlich model may be written as follows:

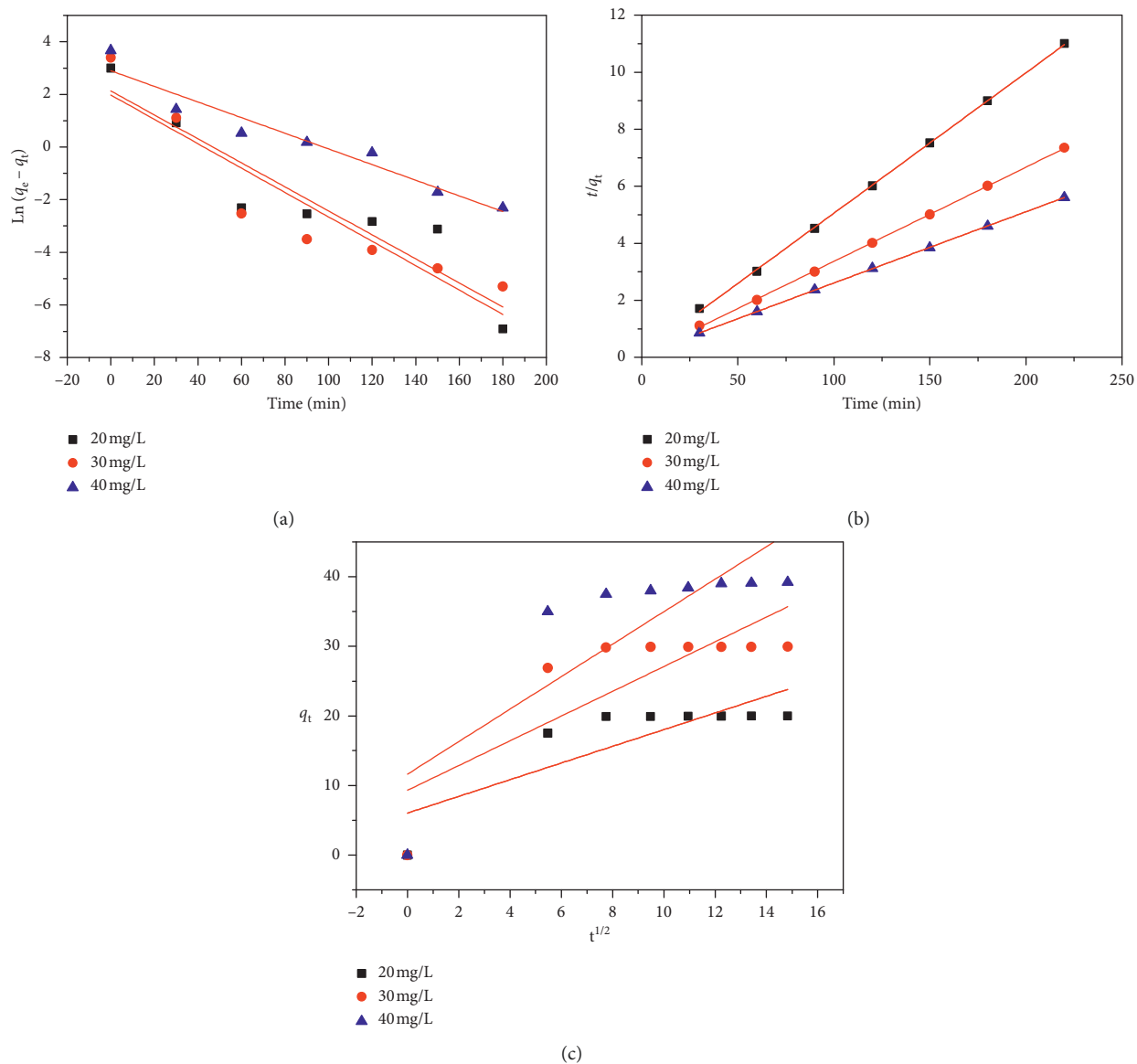


FIGURE 7: Pseudo-first-order (a), Pseudo-second-order (b), and Intraparticle diffusion (c) plots for adsorption of MB by geopolimer.

TABLE 5: Kinetic parameters for the adsorption of MB on geopolimer.

Dye C_0 (mg/L)	Pseudo-first-order				Pseudo-second-order			Intraparticle diffusion model		
	q_{exp}	q_e (mg/g)	k_1 (1/min)	R_1^2	q_e (mg/g)	k_2 (g/mg min)	R_2^2	I (mg/g)	k_{id} (mg/g min ^{0.5})	R_3^2
20	19.99	8.43	0.045	0.875	20.41	0.031	0.999	6.042	1.198	0.683
30	29.93	7.21	0.046	0.866	30.30	0.028	0.999	9.309	1.778	0.669
40	39.2	18.17	0.029	0.936	40	0.0098	0.999	11.64	2.334	0.692

$$\ln q_e = \ln K_F + \frac{1}{n} \ln C_e, \quad (9)$$

where K_F ($\text{mg}^{(1-n)}\text{L}^n\text{g}^{-1}$) is the adsorption capacity and $1/n$ is the adsorption intensity.

3.5. *Dubinin-Radushkevich (D-R) Isotherm.* The D-R isotherm model is a simple model applied to explain the nature of adsorption on the homogeneous or

heterogeneous surface of an adsorbent and validated in high concentrations of adsorbate to determine the type of adsorption (physical or chemical) [63–65]. The simplified D-R isotherm equation is expressed as follows:

$$\ln q_e = \ln(q_m) - K\varepsilon^2, \quad (10)$$

where K is the D-R constant of the sorption energy (mol^2/kJ^2) and ε is the Polanyi potential which is given by

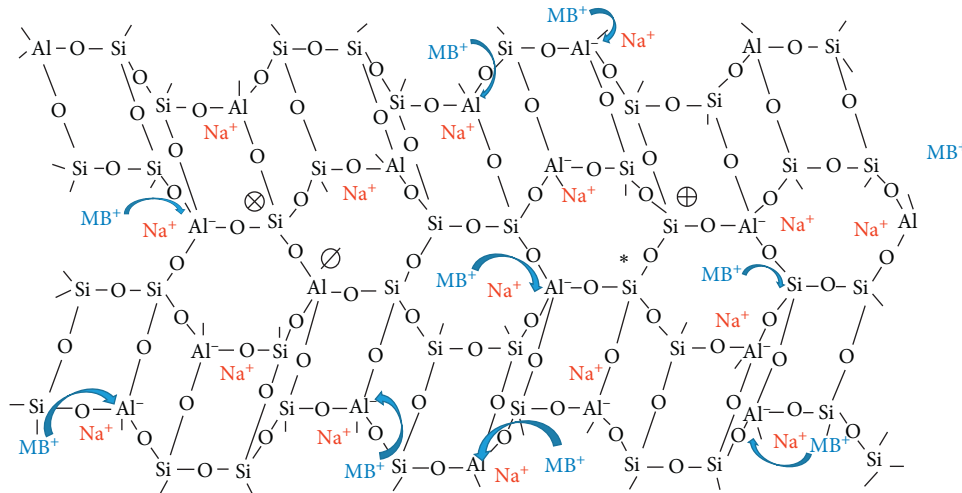


FIGURE 8: Proposed mechanism for adsorption of methylene blue by geopolymer.

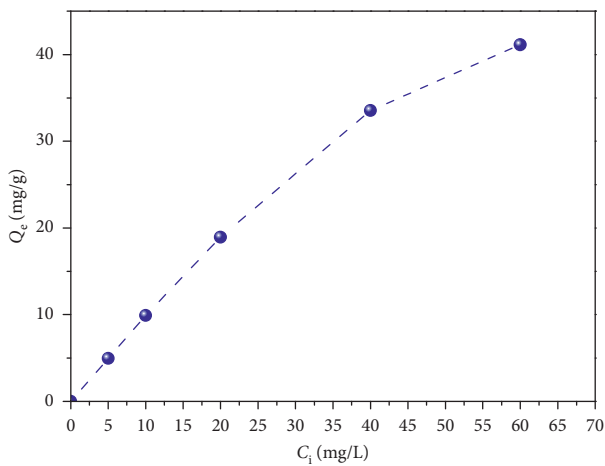


FIGURE 9: Effect of initial MB concentration on adsorption capacity of dye on geopolymer.

TABLE 6: Adsorption properties according to R_L value.

R_L	Information about adsorption
$R_L = 0$	Irreversible
$0 < R_L < 1$	Favorable
$R_L = 1$	Linear
$R_L > 1$	Unfavorable

$$\varepsilon = RT \ln \left(1 + \frac{1}{C_e} \right), \quad (11)$$

where T is the temperature (K), R is the gas constant ($8.314 \text{ J} \cdot \text{mol}^{-1} \cdot \text{K}^{-1}$), C_e (mg/L) is the equilibrium concentration of MB left in solution, and q_m is the D-R maximum adsorption capacity.

The value mean energy of sorption, E (kJ/mol), equation can be calculated from D-R parameter K as follows:

$$E = \frac{1}{\sqrt{(2K)}}. \quad (12)$$

The value of E is useful for estimating the mechanism of the adsorption reaction (chemical or physical adsorption). The value of E between 1 kJ/mol and 8 kJ/mol corresponds to physical adsorption, the E value between 8 and 16 kJ/mol corresponds to adsorption by chemisorption, and when the value of E is greater than 16 kJ/mol, adsorption may be dominated by particle diffusion [66, 67].

3.6. Temkin Isotherm. The Temkin isotherm assumes that the sorption decreases linearly when the interaction between the surface of the adsorbent and adsorbate increases. The linear Temkin model has been used in the following form [68]:

$$q_e = B_T \ln A_T + B_T \ln C_e, \quad (13)$$

where $B_T = R_T/b_T$, b_T is the Temkin constant related to heat of sorption (J/mol), A_T is the Temkin isotherm constant (L/g), R is the universal gas constant ($8.314 \text{ J/mol} \cdot \text{K}$), and T is the temperature (K).

Figure 10 represents the Langmuir, Freundlich, Temkin, and Dubinin–Radushkevich isotherm models. The constants calculated from the model equations (Langmuir, Freundlich, Temkin, and Dubinin–Radushkevich isotherm) are shown in Table 7. As observed, the value of R^2 obtained from the Langmuir isotherm equation (0.994) was higher than that from the Freundlich (0.963), Dubinin–Radushkevich (0.915) and Temkin (0.980) isotherm equations. These results showed that the adsorption experiments data could be well described by the Langmuir model. The adsorption occurred on the homogeneous surface as a monolayer, and the maximum monolayer adsorption capacity (q_{\max}) was found to be 43.48 mg/g. The R_L value was obtained within the range $0 < R_L < 1$, indicating that the adsorption of cationic dye on the geopolymer material is favorable. In addition, Table 8 presents a summary of the maximum adsorption capacity q_{\max} of the developed adsorbents for MB dyestuff in the aqueous medium. A comparison with other reported adsorbents showed that the q_{\max} value for the geopolymer used

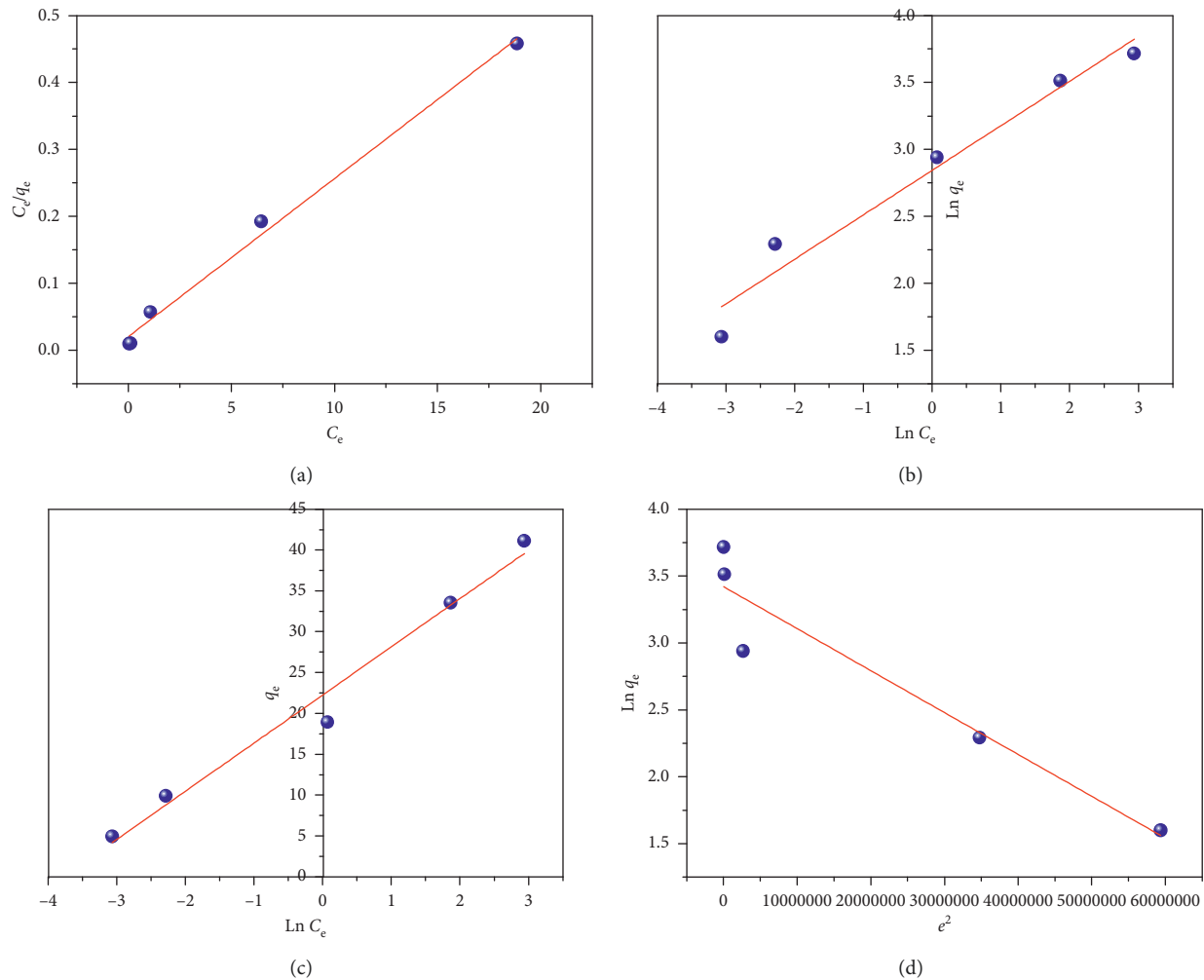


FIGURE 10: Langmuir (a), Freundlich (b), Temkin (c), and Dubinin–Radushkevich (d) isotherms for adsorption of MB by geopolymer.

TABLE 7: Models isotherm constants for adsorption of MB using adsorbent.

Langmuir			Freundlich				Temkin			Dubinin–Radushkevich		
Q_m (mg/g)	K_L (L/mg)	R^2	Range R_L	K_F (mg ⁽¹⁻ⁿ⁾ L ⁿ /g)	$1/n$	R^2	A_T (L/g)	B_T	R^2	Q_m (mg/g)	R^2	E (KJ/mol)
43.48	1.15	0.994	0.014–0.15	17.18	0.332	0.963	43.38	5.897	0.980	30.57	0.915	5.77

TABLE 8: Comparison of the obtained adsorption capacity with the previously developed adsorbents in the literature.

Adsorbents	q_{max} (mg/g)	References
Kaolin geopolymer	25.6	[69]
Phosphoric acid-based geopolymers	4.26	[50]
fly ash-derived zeolites	12.64	[70]
Cold plasma-modified kaolin	23	[71]
Coal fly ash-based geopolymer	50.7	[72]
Fly ash-based geopolymer	37.04	[73]
Biomass FA-geopolymer	15.4	[74]
NaOH-treated raw kaolin	16.34	[75]
Metakaolin-based geopolymer	43.48	Present work

in this study is the highest, indicating that this new solid is an excellent adsorbent for the treatment of water containing MB dye.

3.6.1. *Thermodynamic of Adsorption.* Thermodynamic parameters have an important role to evaluate the phenomenon of the adsorption process. The thermodynamic parameters, namely, free energy (ΔG°), enthalpy (ΔH°), and entropy (ΔS°), for adsorption process were obtained using the following equations [76]:

$$\Delta G^\circ = -RT \ln \frac{q_e}{C_e},$$

$$K_d = \frac{q_e}{C_e}, \quad (14)$$

$$\ln K_d = \frac{\Delta S^\circ}{R} - \frac{\Delta H^\circ}{RT},$$

where q_e is the amount of dye adsorbed per unit mass of the adsorbent at equilibrium (mg/g), C_e is the equilibrium

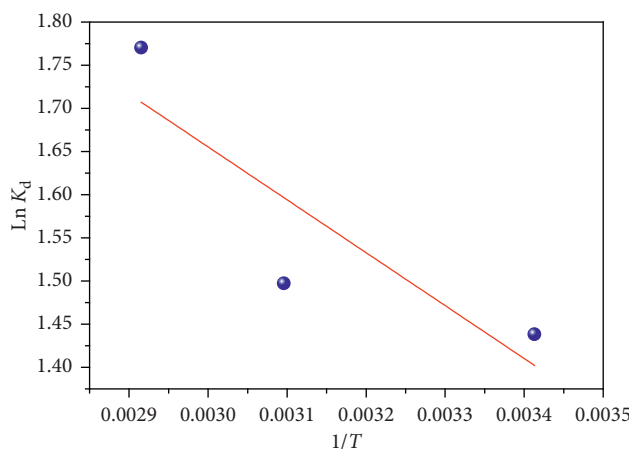


FIGURE 11: Enthalpy and entropy change determination of the adsorption of MB by geopolymer.

TABLE 9: Thermodynamic parameters for the adsorption of MB onto geopolymer.

Adsorbent	Adsorbate	ΔH° (KJ·mol ⁻¹)	ΔS° (KJ·mol ⁻¹ ·K ⁻¹)	ΔG° (KJ·mol ⁻¹)		
				293 K	323 K	343 K
Geopolymer	MB	5.1	0.03	-3.503	-4.021	-5.048

concentration (mg/L), R is the universal gas constant (8.314 J·mol⁻¹·K⁻¹), and T is the solution temperature (K).

The values of enthalpy (ΔH°) and entropy (ΔS°) were calculated from the slope and intercept of the plot of $\ln K_d$ versus $1/T$ (Figure 11). The thermodynamic parameters for methylene blue adsorption on the composite adsorbent at various temperatures are summarized in Table 9. The positive values of entropy (ΔS°) indicate a random increase during adsorption. The negative values of enthalpy ΔH° indicate the endothermic nature of the process. Moreover, the values of ΔG° determined are negative, thus confirming that the adsorption process is spontaneous and thermodynamically favorable. A similar phenomenon has been observed in the adsorption of MB on pomegranate peel activated carbon [77].

4. Conclusion

In summary, a metakaolin-based geopolymer was produced from metakaolin and alkali activators and used as an adsorbent for cationic dye removal. XRF, XRD, FTIR, and SEM studies show that a geoadsorbent was formed by the geopolymerization process. The optimum conditions of adsorption by geopolymer were found to be a geopolymer mass of 0.1 g in 100 mL of MB, an initial concentration of MB 40 mg/L, a contact time of 120 min, and a basic pH. The kinetics study of initial concentration demonstrated that adsorption equilibrium was found to follow the pseudo-second-order equation. The isotherm models data were better described by Langmuir isotherm equation with a maximum monolayer adsorption capacity of 43.48 mg/g. The values of the thermodynamic parameters indicated that the adsorption was spontaneous and endothermic in nature. The overall results prove that the geopolymer has a great potential and a high selectivity and can be considered

an economical adsorbent for the elimination of methylene blue from aqueous medium by batch operation.

Data Availability

The data used to support the findings of this study are available from the corresponding author upon request.

Conflicts of Interest

The authors declare that they have no conflicts of interest.

References

- [1] J. Pang, F. Fu, Z. Ding, J. Lu, N. Li, and B. Tang, "Adsorption behaviors of methylene blue from aqueous solution on mesoporous birnessite," *Journal of the Taiwan Institute of Chemical Engineers*, vol. 77, pp. 168–176, 2017.
- [2] M. Rezaei and S. Salem, "Photocatalytic activity enhancement of anatase-graphene nanocomposite for methylene removal: degradation and kinetics," *Spectrochimica Acta Part A: Molecular and Biomolecular Spectroscopy*, vol. 167, pp. 41–49, 2016.
- [3] S. Khan and A. Malik, "Environmental and health effects of textile industry wastewater," in *Environmental Deterioration and Human Health*, A. Malik, E. Grohmann, and R. Akhtar, Eds., Springer, Dordrecht, Netherlands, pp. 55–71, 2014.
- [4] A. Pandey, P. Singh, and L. Iyengar, "Bacterial decolorization and degradation of azo dyes," *International Biodeterioration & Biodegradation*, vol. 59, no. 2, pp. 73–84, 2007.
- [5] M. Rafatullah, O. Sulaiman, R. Hashim, and A. Ahmad, "Adsorption of methylene blue on low-cost adsorbents: a review," *Journal of Hazardous Materials*, vol. 177, no. 1–3, pp. 70–80, 2010.
- [6] B. Shi, G. Li, D. Wang, C. Feng, and H. Tang, "Removal of direct dyes by coagulation: the performance of preformed polymeric aluminum species," *Journal of Hazardous Materials*, vol. 143, no. 1–2, pp. 567–574, 2007.

- [7] N. Nasuha, S. Ismail, and B. H. Hameed, "Activated electric arc furnace slag as an efficient and reusable heterogeneous fenton-like catalyst for the degradation of reactive black 5," *Journal of the Taiwan Institute of Chemical Engineers*, vol. 67, pp. 235–243, 2016.
- [8] Y. Zhang and L. Liu, "Fly ash-based geopolymers as a novel photocatalyst for degradation of dye from wastewater," *Particuology*, vol. 11, no. 3, pp. 353–358, 2013.
- [9] D. Jellouli Ennigrou, L. Gzara, M. Ramzi Ben Romdhane, and M. Dhahbi, "Cadmium removal from aqueous solutions by polyelectrolyte enhanced ultrafiltration," *Desalination*, vol. 246, no. 1–3, pp. 363–369, 2009.
- [10] A. Dębrowski, Z. Hubicki, P. Podkościelny, and E. Robens, "Selective removal of the heavy metal ions from waters and industrial wastewaters by ion-exchange method," *Chemosphere*, vol. 56, no. 2, pp. 91–106, 2004.
- [11] I. Sirés and E. Brillas, "Remediation of water pollution caused by pharmaceutical residues based on electrochemical separation and degradation technologies: a review," *Environment International*, vol. 40, pp. 212–229, 2012.
- [12] M. El Alouani, S. Alehyen, M. E. Achouri, and M. Taibi, "Potential use of moroccan fly ash as low cost adsorbent for the removal of two anionic dyes (indigo carmine and acid orange)," *Journal of Materials and Environmental Sciences*, vol. 8, pp. 3397–3409, 2017.
- [13] R. Hazzaa and M. Hussein, "Adsorption of cationic dye from aqueous solution onto activated carbon prepared from olive stones," *Environmental Technology & Innovation*, vol. 4, pp. 36–51, 2015.
- [14] Y. Liu, Y. Jiang, M. Hu, S. Li, and Q. Zhai, "Removal of triphenylmethane dyes by calcium carbonate-lentian hierarchical mesoporous hybrid materials," *Chemical Engineering Journal*, vol. 273, pp. 371–380, 2015.
- [15] M. Zbair, Z. Anfar, H. Khallok, H. A. Ahsaine, M. Ezahri, and N. Elalem, "Adsorption kinetics and surface modeling of aqueous methylene blue onto activated carbonaceous wood sawdust," *Fullerenes, Nanotubes and Carbon Nanostructures*, vol. 26, no. 7, pp. 433–442, 2018.
- [16] Y. C. Wong, Y. S. Szeto, W. H. Cheung, and G. McKay, "Equilibrium studies for acid dye adsorption onto chitosan," *Langmuir*, vol. 19, no. 19, pp. 7888–7894, 2003.
- [17] L. Bulgariu, L. B. Escudero, O. S. Bello et al., "The utilization of leaf-based adsorbents for dyes removal: a review," *Journal of Molecular Liquids*, vol. 276, pp. 728–747, 2019.
- [18] K. Rida, S. Bouraoui, and S. Hadnine, "Adsorption of methylene blue from aqueous solution by kaolin and zeolite," *Applied Clay Science*, vol. 83–84, pp. 99–105, 2013.
- [19] V. K. Gupta, R. Jain, M. N. Siddiqui et al., "Equilibrium and thermodynamic studies on the adsorption of the dye rhodamine-B onto mustard cake and activated carbon," *Journal of Chemical & Engineering Data*, vol. 55, no. 11, pp. 5225–5229, 2010.
- [20] H. Deng, L. Yang, G. Tao, and J. Dai, "Preparation and characterization of activated carbon from cotton stalk by microwave assisted chemical activation-application in methylene blue adsorption from aqueous solution," *Journal of Hazardous Materials*, vol. 166, no. 2–3, pp. 1514–1521, 2009.
- [21] S. Bentahar, A. Dbik, M. E. Khomri, N. E. Messaoudi, and A. Lacherai, "Adsorption of methylene blue, crystal violet and congo red from binary and ternary systems with natural clay: kinetic, isotherm, and thermodynamic," *Journal of Environmental Chemical Engineering*, vol. 5, no. 6, pp. 5921–5932, 2017.
- [22] W. Zhao, X. Huang, Y. Wang, S. Sun, and C. Zhao, "A recyclable and regenerable magnetic chitosan adsorbent for dye uptake," *Carbohydrate Polymers*, vol. 150, pp. 201–208, 2016.
- [23] S. Shakoor and A. Nasar, "Removal of methylene blue dye from artificially contaminated water using citrus limetta peel waste as a very low cost adsorbent," *Journal of the Taiwan Institute of Chemical Engineers*, vol. 66, pp. 154–163, 2016.
- [24] J. Sheng, Y. Xie, and Y. Zhou, "Adsorption of methylene blue from aqueous solution on pyrophyllite," *Applied Clay Science*, vol. 46, no. 4, pp. 422–424, 2009.
- [25] Z. Liang, Z. Zhao, T. Sun, W. Shi, and F. Cui, "Enhanced adsorption of the cationic dyes in the spherical CuO/mesoporous silica nano composite and impact of solution chemistry," *Journal of Colloid and Interface Science*, vol. 485, pp. 192–200, 2017.
- [26] Z. Li, G. Wang, K. Zhai, C. He, Q. Li, and P. Guo, "Methylene blue adsorption from aqueous solution by loofah sponge-based porous carbons," *Colloids and Surfaces A: Physicochemical and Engineering Aspects*, vol. 538, pp. 28–35, 2018.
- [27] J. Chang, J. Ma, Q. Ma et al., "Adsorption of methylene blue onto Fe₃O₄/activated montmorillonite nanocomposite," *Applied Clay Science*, vol. 119, pp. 132–140, 2016.
- [28] A. A. Siyal, M. R. Shamsuddin, M. I. Khan et al., "A review on geopolymers as emerging materials for the adsorption of heavy metals and dyes," *Journal of Environmental Management*, vol. 224, pp. 327–339, 2018.
- [29] J. Davidovits, "Geopolymers," *Journal of Thermal Analysis*, vol. 37, no. 8, pp. 1633–1656, 1991.
- [30] J. Temuujin, R. P. Williams, and A. van Riessen, "Effect of mechanical activation of fly ash on the properties of geopolymer cured at ambient temperature," *Journal of Materials Processing Technology*, vol. 209, no. 12–13, pp. 5276–5280, 2009.
- [31] T. R. Barbosa, E. L. Foletto, G. L. Dotto, and S. L. Jahn, "Preparation of mesoporous geopolymer using metakaolin and rice husk ash as synthesis precursors and its use as potential adsorbent to remove organic dye from aqueous solutions," *Ceramics International*, vol. 44, no. 1, pp. 416–423, 2018.
- [32] Y. J. Zhang, L. C. Liu, Y. Xu, Y. C. Wang, and D. L. Xu, "A new alkali-activated steel slag-based cementitious material for photocatalytic degradation of organic pollutant from waste water," *Journal of Hazardous Materials*, vol. 209–210, pp. 146–150, 2012.
- [33] S. Alehyen, M. Zerzouri, M. EL Alouani, M. EL Achouri, and M. Taibi, "Porosity and fire resistance of fly ash based geopolymer," *Journal of Materials and Environmental Sciences*, vol. 9, pp. 3676–3689, 2017.
- [34] R. R. Pawar, B. H. C. Lalhmunsiam, H. C. Bajaj, and S.-M. Lee, "Activated bentonite as a low-cost adsorbent for the removal of Cu(II) and Pb(II) from aqueous solutions: batch and column studies," *Journal of Industrial and Engineering Chemistry*, vol. 34, pp. 213–223, 2016.
- [35] G. S. Ryu, Y. B. Lee, K. T. Koh, and Y. S. Chung, "The mechanical properties of fly ash-based geopolymer concrete with alkaline activators," *Construction and Building Materials*, vol. 47, pp. 409–418, 2013.
- [36] Q. Wan, F. Rao, S. Song, D. F. Cholíco-González, and N. L. Ortiz, "Combination formation in the reinforcement of metakaolin geopolymers with quartz sand," *Cement and Concrete Composites*, vol. 80, pp. 115–122, 2017.
- [37] M. Jin, Z. Zheng, Y. Sun, L. Chen, and Z. Jin, "Resistance of metakaolin-MSWI fly ash based geopolymer to acid and

- alkaline environments,” *Journal of Non-Crystalline Solids*, vol. 450, pp. 116–122, 2016.
- [38] F. G. M. Aredes, T. M. B. Campos, J. P. B. Machado, K. K. Sakane, G. P. Thim, and D. D. Brunelli, “Effect of cure temperature on the formation of metakaolinite-based geopolymer,” *Ceramics International*, vol. 41, no. 6, pp. 7302–7311, 2015.
- [39] J. C. Swanepoel and C. A. Strydom, “Utilisation of fly ash in a geopolymeric material,” *Applied Geochemistry*, vol. 17, no. 8, pp. 1143–1148, 2002.
- [40] A. Boukhemkhem and K. Rida, “Improvement adsorption capacity of methylene blue onto modified tamazert kaolin,” *Adsorption Science & Technology*, vol. 35, no. 9–10, pp. 753–773, 2017.
- [41] N. Belmokhtar, M. Ammari, J. Brigui, and L. Ben Allal, “Comparison of the microstructure and the compressive strength of two geopolymers derived from metakaolin and an industrial sludge,” *Construction and Building Materials*, vol. 146, pp. 621–629, 2017.
- [42] C. M. Müller, B. Pejčić, L. Esteban, C. D. Piane, M. Raven, and B. Mizaikoff, “Infrared attenuated total reflectance spectroscopy: an innovative strategy for analyzing mineral components in energy relevant systems,” *Scientific Reports*, vol. 4, no. 1, p. 6764, 2014.
- [43] T. Bakharev, “Resistance of geopolymer materials to acid attack,” *Cement and Concrete Research*, vol. 35, no. 4, pp. 658–670, 2005.
- [44] W. K. W. Lee and J. S. J. van Deventer, “The effects of inorganic salt contamination on the strength and durability of geopolymers,” *Colloids and Surfaces A: Physicochemical and Engineering Aspects*, vol. 211, no. 2–3, pp. 115–126, 2002.
- [45] İ. Kara, D. Yilmazer, and S. T. Akar, “Metakaolin based geopolymer as an effective adsorbent for adsorption of zinc(II) and nickel(II) ions from aqueous solutions,” *Applied Clay Science*, vol. 139, pp. 54–63, 2017.
- [46] D. Krizan and B. Zivanovic, “Effects of dosage and modulus of water glass on early hydration of alkali-slag cements,” *Cement and Concrete Research*, vol. 32, no. 8, pp. 1181–1188, 2002.
- [47] L. Chen, Z. Wang, Y. Wang, and J. Feng, “Preparation and properties of alkali activated metakaolin-based geopolymer,” *Materials*, vol. 9, no. 9, p. 767, 2016.
- [48] C. P. J. Isaac and A. Sivakumar, “Removal of lead and cadmium ions from water using *Annona squamosa* shell: kinetic and equilibrium studies,” *Desalination and Water Treatment*, vol. 51, no. 40–42, pp. 7700–7709, 2013.
- [49] A. Maleki, M. Mohammad, Z. Emdadi, N. Asim, M. Azizi, and J. Safaei, “Adsorbent materials based on a geopolymer paste for dye removal from aqueous solutions,” *Arabian Journal of Chemistry*, 2018, In press.
- [50] M. I. Khan, T. K. Min, K. Azizli, S. Sufian, H. Ullah, and Z. Man, “Effective removal of methylene blue from water using phosphoric acid based geopolymers: synthesis, characterizations and adsorption studies,” *RSC Advances*, vol. 5, no. 75, pp. 61410–61420, 2015.
- [51] D. Kavitha and C. Namasivayam, “Experimental and kinetic studies on methylene blue adsorption by coir pith carbon,” *Bioresource Technology*, vol. 98, no. 1, pp. 14–21, 2007.
- [52] S. M. de Oliveira Brito, H. M. C. Andrade, L. F. Soares, and R. P. de Azevedo, “Brazil nut shells as a new biosorbent to remove methylene blue and indigo carmine from aqueous solutions,” *Journal of Hazardous Materials*, vol. 174, no. 1–3, pp. 84–92, 2010.
- [53] S. A. Hamid, M. Shahadat, and S. Ismail, “Development of cost effective bentonite adsorbent coating for the removal of organic pollutant,” *Applied Clay Science*, vol. 149, pp. 79–86, 2017.
- [54] S. Lagergren, “Zur theorie der sogenannten adsorption geloster stoffe,” *Kungliga Svenska Vetenskapsakademiens Handlingar*, vol. 24, pp. 1–39, 1898.
- [55] Y. S. Ho and G. McKay, “Pseudo-second order model for sorption processes,” *Process Biochemistry*, vol. 34, no. 5, pp. 451–465, 1999.
- [56] J. F. Baret, “Kinetics of adsorption from a solution. Role of the diffusion and of the adsorption-desorption antagonism,” *Journal of Physical Chemistry*, vol. 72, no. 8, pp. 2755–2758, 1968.
- [57] A. Baraka, “Adsorptive removal of tartrazine and methylene blue from wastewater using melamine-formaldehyde-tartaric acid resin (and a discussion about pseudo second order model),” *Desalination and Water Treatment*, vol. 44, no. 1–3, pp. 128–141, 2012.
- [58] J. Hu, W. Dai, and X. Yan, “Comparison study on the adsorption performance of methylene blue and congo red on Cu-BTC,” *Desalination and Water Treatment*, vol. 57, no. 9, pp. 4081–4089, 2016.
- [59] X. Peng, D. Huang, T. Odoom-Wubah, D. Fu, J. Huang, and Q. Qin, “Adsorption of anionic and cationic dyes on ferromagnetic ordered mesoporous carbon from aqueous solution: equilibrium, thermodynamic and kinetics,” *Journal of Colloid and Interface Science*, vol. 430, pp. 272–282, 2014.
- [60] D. Singh, S. K. Singh, N. Atar, and V. Krishna, “Amino acid functionalized magnetic nanoparticles for removal of Ni(II) from aqueous solution,” *Journal of the Taiwan Institute of Chemical Engineers*, vol. 67, pp. 148–160, 2016.
- [61] T. W. Weber and R. K. Chakravorty, “Pore and solid diffusion models for fixed-bed adsorbers,” *AIChE Journal*, vol. 20, no. 2, pp. 228–238, 1974.
- [62] H. Freundlich and W. Heller, “The Adsorption of cis- and trans-azobenzene,” *Journal of the American Chemical Society*, vol. 61, no. 8, pp. 2228–2230, 1939.
- [63] M. M. Dubinin, E. Zaverina, and L. Radushkevich, “Sorption and structure of active carbons. I. Adsorption of organic vapors,” *Zhurnal Fizicheskoi Khimii*, vol. 21, pp. 151–162, 1947.
- [64] F. Ouadjenia-Marouf, R. Marouf, J. Schott, and A. Yahiaoui, “Removal of Cu(II), Cd(II) and Cr(III) ions from aqueous solution by dam silt,” *Arabian Journal of Chemistry*, vol. 6, no. 4, pp. 401–406, 2013.
- [65] H. Zheng, D. Liu, Y. Zheng, S. Liang, and Z. Liu, “Sorption isotherm and kinetic modeling of aniline on Cr-bentonite,” *Journal of Hazardous Materials*, vol. 167, no. 1–3, pp. 141–147, 2009.
- [66] K. Saltalı, A. Sarı, and M. Aydın, “Removal of ammonium ion from aqueous solution by natural Turkish (Yıldızeli) zeolite for environmental quality,” *Journal of Hazardous Materials*, vol. 141, pp. 258–263, 2007.
- [67] A. Sarı, M. Tuzen, D. Çitak, and M. Soylak, “Adsorption characteristics of Cu(II) and Pb(II) onto expanded perlite from aqueous solution,” *Journal of Hazardous Materials*, vol. 148, pp. 387–394, 2007.
- [68] F. Rozada, M. Otero, A. I. García, and A. Morán, “Application in fixed-bed systems of adsorbents obtained from sewage sludge and discarded tyres,” *Dyes and Pigments*, vol. 72, no. 1, pp. 47–56, 2007.
- [69] R. I. Yousef, B. El-Eswed, M. Alshaaer, F. Khalili, and H. Khoury, “The influence of using Jordanian natural zeolite on the adsorption, physical, and mechanical properties of

- geopolymers products,” *Journal of Hazardous Materials*, vol. 165, no. 1-3, pp. 379–387, 2009.
- [70] C. D. Woolard, J. Strong, and C. R. Erasmus, “Evaluation of the use of modified coal ash as a potential sorbent for organic waste streams,” *Applied Geochemistry*, vol. 17, no. 8, pp. 1159–1164, 2002.
- [71] Ö. Yavuz and C. Saka, “Surface modification with cold plasma application on kaolin and its effects on the adsorption of methylene blue,” *Applied Clay Science*, vol. 85, pp. 96–102, 2013.
- [72] Y. Liu, C. Yan, Z. Zhang, Y. Gong, H. Wang, and X. Qiu, “A facile method for preparation of floatable and permeable fly ash-based geopolymer block,” *Materials Letters*, vol. 185, pp. 370–373, 2016.
- [73] M. EL Alouani, S. Alehyen, M. EL Achouri, and M. Taibi, “Removal of cationic dye—methylene blue—from aqueous solution by adsorption on fly ash—based geopolymer,” *Journal of Materials and Environmental Sciences*, vol. 9, no. 1, pp. 32–46, 2018.
- [74] R. M. Novais, G. Ascensão, D. M. Tobaldi, M. P. Seabra, and J. A. Labrincha, “Biomass fly ash geopolymer monoliths for effective methylene blue removal from wastewaters,” *Journal of Cleaner Production*, vol. 171, pp. 783–794, 2018.
- [75] D. Ghosh and K. G. Bhattacharyya, “Adsorption of methylene blue on kaolinite,” *Applied Clay Science*, vol. 20, no. 6, pp. 295–300, 2002.
- [76] S. A. Drweesh, N. A. Fathy, M. A. Wahba et al., “Equilibrium, kinetic and thermodynamic studies of Pb(II) adsorption from aqueous solutions on HCl-treated Egyptian kaolin,” *Journal of Environmental Chemical Engineering*, vol. 4, no. 2, pp. 1674–1684, 2016.
- [77] M. A. Ahmad, N. A. Ahmad Puad, and O. S. Bello, “Kinetic, equilibrium and thermodynamic studies of synthetic dye removal using pomegranate peel activated carbon prepared by microwave-induced KOH activation,” *Water Resources and Industry*, vol. 6, pp. 18–35, 2014.